Thi Bich Van Pham MSc

Dependence of Initial Quenching Products and Exciplex Kinetics on Polar Components in Binary Solvents Investigated by Time-Resolved Magnetic Field Effects on Exciplexes

DISSERTATION

zur Erlangung des akademischen Grades
Doktor der Naturwissenschaften
eingereicht an der

Technischen Universität Graz

Betreuer
O. Univ.-Prof. Dipl.-Chem. Dr. Günter Grampp
Institut für Physikalische und Theoretische Chemie

Graz, Jänner 2015

EIDESSTATTLICHE ERKLÄRUNG
AFFIDAVIT

Ich erkläre an Eides statt, dass ich die vorliegende Arbeit selbstständig verfasst, andere als die angegebenen Quellen/Hilfsmittel nicht benutzt, und die den benutzten Quellen wörtlich und inhaltlich entnommenen Stellen als solche kenntlich gemacht habe. Das in TUGRAZonline hochgeladene Textdokument ist mit der vorliegenden Dissertation identisch.

I declare that I have authored this thesis independently, that I have not used other than the declared sources/resources, and that I have explicitly indicated all material which has been quoted either literally or by content from the sources used. The text document uploaded to TUGRAZ online is identical to the present doctoral dissertation.

_____ _____

Datum / Date Unterschrift / Signature

to Hoàng Minh Đăng

to my parents

CONTENTS

LIST OF FIGURES

LIST OF TABLES

ABSTRACT

By designing solvent mixtures from micro-homogeneous to micro-heterogeneous environments, the effect of polarity scan and polar components in binary solvents on the initial quenching products (exciplexes versus loose ion pairs) and exciplex kinetics has been studied on the system 9,10-dimethylanthracene (fluorophore)/*N*,*N*-dimethylaniline (quencher). Time-resolved MFEs (TR-MFE) on the exciplex emission of fluorophore/quencher pair were observed using the Time-Correlated Single Photon-Counting (TCSPC) approach in the absence and presence of a saturating external magnetic field. The bulk dielectric constants, ε_s, of micro-homogeneous solvent mixtures of propyl acetate/butyronitrile were varied within a range from 6 to 24.7, while those of micro-heterogeneous media of toluene/dimethylsulfoxide were in the range from 4.3 to 15.5. In the micro-heterogeneous solutions, the TR-MFEs of the exciplex emission occur at a shorter timescale in comparison to the iso-dielectric micro-homogeneous solvents. Simulations of TR-MFE experimental data indicate the role of polar components on distinguishing exciplexes from loose ion pairs. Furthermore, TR-MFE measurements granted a detailed exciplex kinetics.

ZUSAMMENFASSUNG

Die Effekte von polaren Komponenten in binären Lösungsmitteln auf das anfängliche Quenchprodukt (Exciplexe vs. freie Ionenpaaren) und auf die Exciplexkinetik wurde anhand des Systems 9,10-Dimethylanthrazen (Fluorophor) / *N*,*N*-Dimethylanilin (Quencher) untersucht, indem Lösungsmittelgemische mit unterschiedlichen Eigenschaften (von mikro-homogen zu mikro-heterogen) verwendet wurden. Zeitaufgelöste Magnetfeldeffekte, welche die Exciplex Emission des Fluorophor/Quencher Paares beeinflussen, wurden beobachtet. Diese Messungen wurden mit Hilfe einer zeitkorrelierten Einzelphotonenzählung in An- und Abwesenheit eines externen magnetfeldes durchgeführt. Die statische Dielektrizitätskonstante, ε_s, des mikro-homogenen Lösungsmittelgemisches Propylacetat/Butyronitril wurde zwischen 6 und 24,7 variiert. Die ε_s des mikro-heterogenen Gemisches Toluol/Dimethylsulfoxid wurde 4,3 und 15,5. In den mikro-heterogenen Gemischen sind die zeitaufgelösten Magnetfeldeffekte der Exciplex-Emission auf einer kürzeren Zeitskala beobachtbar als bei iso-dielektrischen mikro-homogenen Gemischen. Simulationen der experimentellen Daten deuten auf eine wichtige Rolle der polaren Komponenten um zwischen Exciplexe und freien Ionenpaaren zu unterscheiden. Außerdem erlaubten diese Messungen eine detaillierte Bestimmung der Exciplexkinetiken.

ACKNOWLEDGEMENTS

I would like to thank:

Dr. Daniel Kattnig, who wrote and helped me on developing the Matlab software for the analysis of the TR-MFE data. For your guidance, detailed explanations relating to my study. I would not accomplish this work without your help. I can never fully express my gratitude and appreciation to you. Thanks!

Prof. Dr. Günter Grampp, my supervisor, who made it possible for me to go to Graz. For your advice and inspiration. For making me feel at home. You made me develop my knowledge in electron transfer and photochemistry theories. Thanks!

Ao. Prof. Dr. Stephan Landgraf, for always being there when I needed help. Thank you for adjusting and fixing the Single Photon Counting apparatus.

Dr. Kenneth Rasmussen, Dr. Boryana Mladenova, who were helpful in science for my work. You gave me honest advices. Our friendship is forever…

Helmuth, Lang and Hilde, for ensuring that the equipment and chemicals run smoothly.

Everybody else at Institute of Physical and Theoretical Chemistry, Graz University of Technology, who I have had the pleasure to know during my stay here. Colleagues, friends. Thanks for your help.

Vietnam International Education Development (VIED) and Austrian Science Foundation, FWF-Project P 21518-N19 for financial support for 3 years.

Hảo, Đăng and my family for their endless love.

1. INTRODUCTION

Solvent polarity dependence of magnetic field effects (MFEs) of the exciplexes has been extensively studied [1-7]. In particular, the presence of polar micro-domains in binary solvents may affect the preferential solvation process of radical ion pairs (RIPs). This results in some interesting phenomena. The $B_{1/2}$ values (the field at which the delayed exciplex emission reaches half its maximum intensity relative to that at zero field) show either a decrease in micro-heterogeneous solvents or remain constant in micro-homogeneous solutions with increasing polarity [2, 4, 6]. These results give the details the solvation dynamics of a RIP in micro-heterogeneous binary solvents. Detailed insights of the exciplex kinetics and the question about the initial quenching products in photo-induced electron transfer (PET) reactions still remain. The solvent polarity strongly affects the mechanism of the fluorescence quenching. In polar solvents (high dielectric constants), quenching occurs by full electron transfer (ET) from quencher (Q) to the photo-excited fluorophore (F*), forming loose ion pairs (LIPs) or radical ion pairs. In non-polar solvents (low dielectric constants), the formation of an excited-state charge transfer complex (exciplex) is often observed, which can dissociate into the RIP and also result from recombination of initially formed ion-pairs. For the solvent of moderate polarity, both quenching reactions may contribute simultaneously and deciding which reaction channel dominates is difficult [8-12]. Any factors imposed on the RIP molecular dynamics may affect MFE features. Thus, the exciplex system can work as a magneto–fluorescent probe [1, 4-7, 13-20]. An external magnetic field will remove the degeneracy of the three triplet sublevels (T_0 and $T_{\pm}$) of spin–correlated RIP generated via photo-induced electron transfer in solution. When the energy separation between three triplet states exceeds the size of the mixing interaction, $T_{\pm}$ cannot mix with the singlet state, S. Thus, the external magnetic field reduces the probability of the intersystem crossing and, therefore, changes relative concentrations of both singlet and triplet states [21-24]. The spin mixing between S and T_0 occurs when the electron exchange interaction depending exponentially on the distance between radical ions and determining the energy gap between S and T_0 levels is less than hyperfine interaction. The singlet RIP concentration can be detected through the emission of the exciplex produced on singlet RIP cage recombination.

There have been several results reported the MFEs on exciplex by time–resolved method to clarify the mechanism of fluorescence quenching, i.e., the initial quenching products are LIPs

or exciplexes. However, these studied have assumed that the LIP is generated first by remote ET and irreversibly re-forms to the exciplex [15, 16, 18, 19, 25-28] or that the exciplex is the primary quenching product even in high polar solution [7, 29, 30]. These approaches would not take the details of exciplex kinetics into account and the reaction mechanism is ambiguous.

As recently shown, time-resolved MFEs of the exciplexes can distinguish the reaction channels (LIPs versus exciplexes). This approach has been conducted in refs. 1, 20. There, solvent polarity and ET driving force dependences of quenching mechanism were clarified by using time-resolved MFE measurements on the exciplex luminescence in micro-homogeneous binary solvents. In present work, the solvent polarity dependence of the MFEs on the exciplex emission is measured in micro-homogeneous (propyl acetate (PA)/butyronitrile (BN)) and micro–heterogeneous (toluene (TOL)/dimethylsulfoxide (DMSO)) binary solvents with varying the static dielectric constants, ε_s. by time–resolved MFEs of the exciplexes based on Time–Correlated Single Photon-Counting (TCSPC) technique. The model which the exciplex dissociation taken into account is used to simulate the experimental data [1, 20]. Time-resolved MFEs allow discriminating the initial reaction products and showing a detailed exciplex kinetics which sensitive to the local dielectric heterogeneities of binary solvents. The results indicated that the presence of high polar components (BN and DMSO) in the solvation shell plays an important role in exciplex kinetics and in deciding the reaction channels. In particular, the much better preferential solvation of DMSO molecules surrounding RIPs and exciplexes results in interesting observations in micro-heterogeneous solutions.

This thesis is organized as follows:

- Theoretical foundations are summarized in chapter 2, including theories of photo-induced electron transfer, magnetic field effects (MFEs) on the exciplexes (time-resolved and steady-state MFEs), solvent models and Time-Correlated Single Photon-Counting (TCSPC) technique.
- Simulation model, solvent and sample preparations, apparatuses and MFE measurements are presented in chapter 3.
- Experimental results are discussed in chapter 4.
- Finally, conclusions and outlooks to possible future work are showed in chapter 5.

2. THEORETICAL FOUNDATIONS

2.1. Photo-induced Electron Transfer

2.1.1. Theories of photo-induced electron transfer

Photo-induced electron transfer (PET) is an attractive area of research in chemistry, physics, and biochemistry [31-34]. In PET reactions, the electron donor or acceptor absorbs the light to an excited state and electron transfer is a one of the ways to deactivate to ground state. Rabinowich has been recognized that, an electronically excited molecule has a tendency to give away an electron as well as accept an electron [35]. This conclusion was quantitatively formulated in the Rehm-Weller equation [36, 37]. According to Rehm-Weller equation, molecules absorb photon to undergo redox reactions, the activation energy being equal to the excitation energy of the molecule from a ground state to an excited state.

Photo-induced electron transfer is a movement of an electron, caused by the absorption of light, from an electron rich molecule (an electron donor-D) to an electron deficient one (an electron acceptor-A). In PET, either a donor, an acceptor, or a ground state complex between the donor and acceptor can absorb photon. A general reaction involving the PET is given in equations (2.1) to (2.3).

$$A \xrightarrow{h\nu} A^{*} \tag{2.1}$$

$$A^{*} + D \xrightarrow{ET} A^{-\cdot} + D^{+\cdot} \tag{2.2}$$

$$A^{-\cdot} + D^{+\cdot} \xrightarrow{RET} A + D \tag{2.3}$$

The molecule absorbs a photon to get into the excited state, referring to as ‘sensitizer’ and the other molecule as the ‘quencher’. A molecule in an excited state can be either in the singlet or in the triplet state. Equation (2.3) gives the return electron transfer (RET) which regenerates the ground states. The electron transfer reaction denoted by equation (2.2) proceeds in several steps. The interaction between A* and D creates a series of short-lived intermediates, each possessing has special geometry and electronic distribution [37, 38].

Figure 2.1 depicts an overall electron transfer reaction. The A* and D approach each other in solution by diffusion to form an encounter complex. A collision complex is formed if further diffusion towards each other. The reactants and intermediates are surrounded by solvent molecules. The sensitizer and quencher are contained within a solvent cage at a centre-to-

centre distance (d_{cc}) of ~7 Å. The lifetimes of these complexes are usually in the 10^{-9}-10^{-11} s range. A contact ion pair (CIP) or exciplex is generated via electron transfer between the A* and D in the collision and encounter complexes. The partners in CIP may be separated by solvent molecules to generate a solvent separated ion pair (SSIP). Finally, the ions in SSIP move apart to form solvated ions (free ions). The CIP and SSIP are sometimes described as geminate ion pairs.

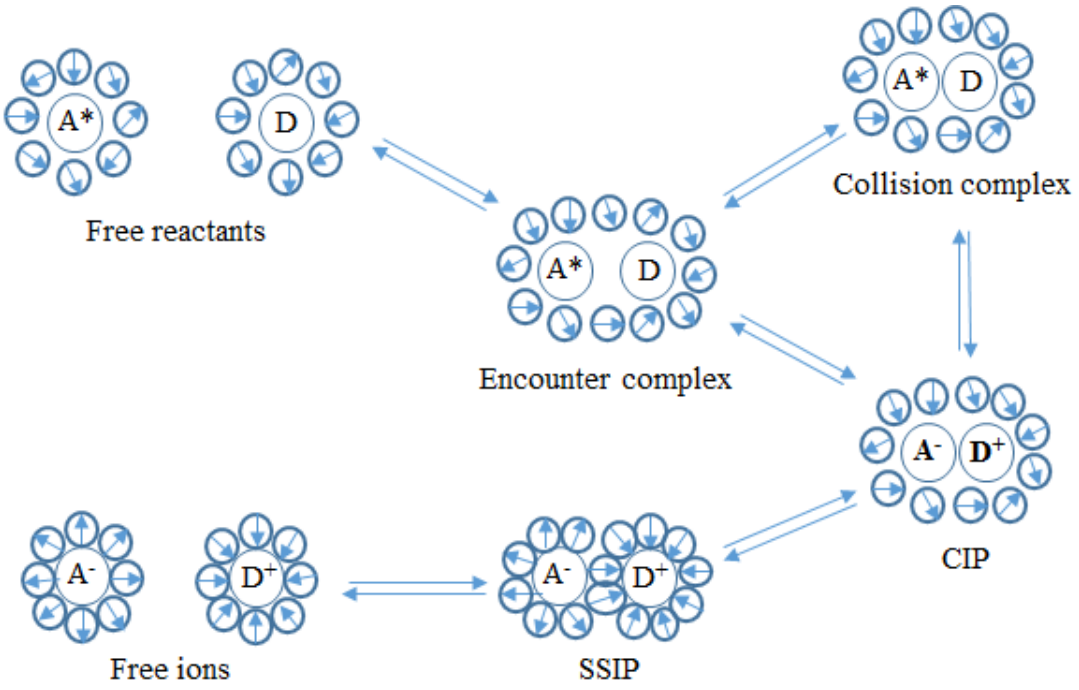

Figure 2.1. The visualization of photo-induced electron transfer reaction.

2.1.2. The role of diffusion

The Smoluchowski's model is normally used to describe the expression for the diffusion rate constant. The model follows some assumptions [39].

1. The size of acceptor (A) and donor (D) are larger than one of solvent molecules and A and D are spherical particles (Figure 2.2).

2. The acceptors arrive to the surface of the donor and react irreversibly with D. The diffusion rate constant $k_d >> k_{-d}$ (Scheme 2.1).

$$A + D \underset{k_{-d}}{\overset{k_d}{\rightleftharpoons}} (A..D) \xrightarrow{k_R} products$$

Scheme 2.1. A and D approach each other by diffusion in solution.

3. The sum of radius of D and A is, $\sigma = r_D + r_A$.

4. Diffusion step determines the reaction rate between A and D ($k_R >> k_d$) (Scheme 2.1).

Molecule A diffuses to a stationary D characterized by diffusion coefficient:

$$D_{diff} = D_{diff}^{A} + D_{diff}^{D} \tag{2.4}$$

Here, D_{diff}^{A} and D_{diff}^{D} are diffusion coefficients of A and D, respectively.

In general, the density distribution of a species A, ρ(r, t), a function of time (t) and distance (r), must obey the diffusion equation [40]:

$$\frac{\delta\rho(r,t)}{\delta t} = (D_{diff}^{A} + D_{diff}^{D})\nabla^2\rho(r,t) + \nabla J_A(r,t) \tag{2.5}$$

Here ∇ is the del operator ($\nabla^2 = \frac{\partial^2}{\partial x^2} + \frac{\partial^2}{\partial y^2} + \frac{\partial^2}{\partial z^2}$); J_A(r, t) is the current density of particles A (The flux of particles A falling to the sink D).

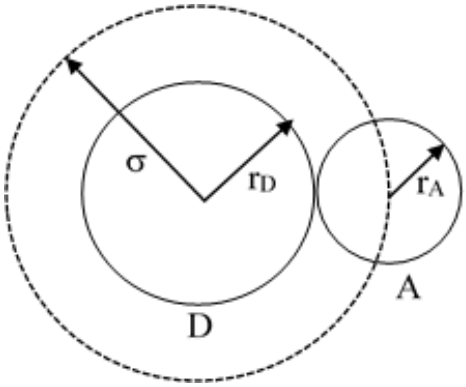

Figure 2.2. The Smoluchowski's model

The flux of particles A is proportional to its density distribution:

$$J_A(r,t) = -w(r,t)\rho(r,t) \tag{2.6}$$

Here the factor $w(r,t)$ is the remote reaction rate.

Introducing eq. (2.6) in eq. (2.5) yields [41, 42].

$$\frac{\delta\rho(r,t)}{\delta t} = (D_{diff}^{A} + D_{diff}^{D})\nabla^2\rho(r,t) + \nabla w(r,t)\rho(r,t) \tag{2.7}$$

With the boundary conditions:

$$\begin{cases} \rho(r,t) = 1 : initial \\ \rho(\sigma,t) = 0 : inner \\ \rho(\infty,t) = 1 : outer \end{cases} \tag{2.8}$$

With an excess of A, the kinetic law for Scheme 2.1 can be expressed:

$$\frac{d[D]}{dt} = -k(t)[D][A]_0 \tag{2.9}$$

$$k(t) = 4\pi\int_{\sigma}^{\infty} w(r,t)\rho(r,t)r^2 dr \tag{2.10}$$

The resulting solution of eq. (2.7), the Smoluchowski diffusion rate constant is obtained:

$$k(t) = 4\pi\sigma D_{diff}(1 + \frac{\sigma}{\sqrt{\pi D_{diff} t}}) \tag{2.11}$$

$t \to \infty$:

$$k(\infty) = 4\pi\sigma D_{diff} \tag{2.12}$$

Using the Stokes-Einstein relation for D_{diff}:

$$D_{diff}^{i} = \frac{k_B T}{6\pi\eta r_i} \tag{2.13}$$

One gets the Einstein-Smoluchowski equation. The rate constant of diffusion is given by:

$$k_d = \frac{2}{3}\frac{k_B T}{\eta}\left(\frac{1}{r_A} + \frac{1}{r_D}\right)\left(r_A + r_D\right) \tag{2.14}$$

Here, η is the solvent viscosity, k_B is the Boltzmann constant and T refers to temperature.

2.1.3. Energetics

The electron transfer between a donor and an acceptor is driven by the change in free energy (driving force), ΔG^0 [43, 44]. An exergonic reaction ($\Delta G^0 < 0$) is required for an efficient quenching process of an excited state.

For a bimolecular electron transfer reaction between two ground-state molecules, the free energy change in the gas phase is calculated by [45]:

$$\Delta G^0 = IP_D - EA_A \tag{2.15}$$

Where IP_D and EA_A are the ionization potential of a donor and the electron affinity of an acceptor, respectively.

Figure 2.3 describes the electron movement from a reactant in excited-state (A* or D*) to one in ground-state in terms of the simplified molecular orbital diagrams. The unoccupied orbital of the acceptor receives an electron from an occupied orbital of the donor in an exothermic process. Thus, one of the reactants in an excited-state results in a reduction in the ionization potential and electron affinity:

$$EA_{A^*} = EA_A + E_{00}^{A \to A^*} \tag{2.16}$$

$$IP_{D^*} = IP_D - E_{00}^{D \to D^*} \tag{2.17}$$

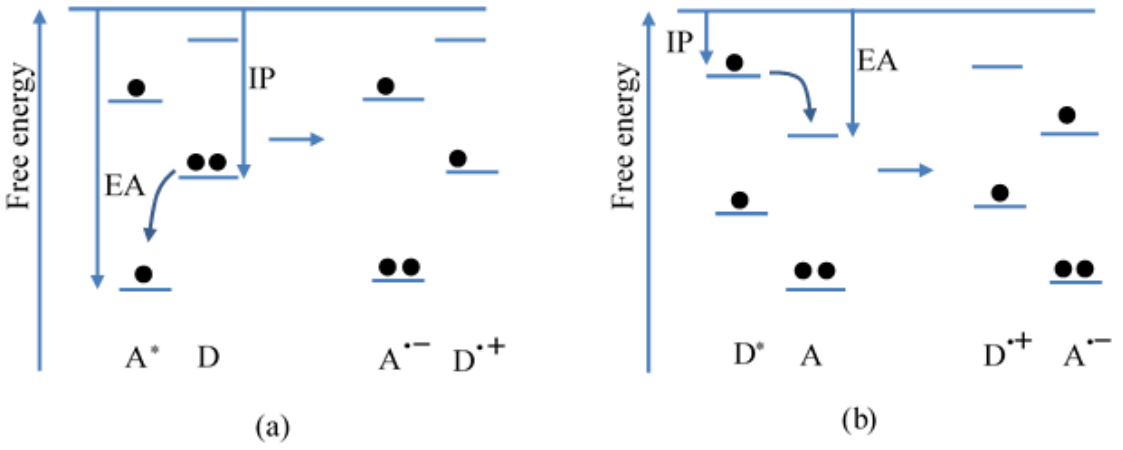

Figure 2.3. The electron movement in an electron transfer process described in terms of the molecular orbital diagrams. A* is an electron acceptor (a) or an electron donor (b).

If the excited-state molecule is an electron donor, eq. (2.15) becomes:

$$\Delta G^0 = IP_D - EA_A - E_{00}^{D \to D^*} \tag{2.18}$$

and the acceptor is electronically excited,

$$\Delta G^0 = IP_D - EA_A - E_{00}^{A \to A^*} \tag{2.19}$$

Equation (2.18) and (2.19) are used only for the PET reaction in the gas phase. When PET occurred in solution, solvation energies (ΔG_{sol}) and Coulombic interaction energies must be taken into account. The free energy change for electron transfer process generating the solvent separated ion pair (ΔG_{SSIP}) is given by:

$$\Delta G_{SSIP}^0 = IP_D - EA_A - E_{00}^{A \to A^*} + \Delta G_{sol} + w_p - w_R \tag{2.20}$$

$E_{00}^{A \to A^*}$ is the 0,0-transition energy. w_P and w_R are the work terms for electrostatic interaction in the product and reactant states, respectively, and are expressed by:

$$w = \frac{z_A z_D e_0^2}{d_{cc} \varepsilon_s} \tag{2.21}$$

Here, z_A, z_D are the charges of the acceptor and donor, respectively, e_0 is the elementary charge d_{cc} is the center-to-center distance and ε_S the solvent dielectric constant. ΔG_{sol} comprises of solvation energies of the ions:

$$\Delta G_{sol} = \Delta G(D^+) + \Delta G(A^-) \tag{2.22}$$

In solution, the ionization potentials of the donor and electron affinities of the acceptor are expressed via redox potentials:

$$IP = E^0(D^+ / D) - \Delta G_{sol} + const \tag{2.23}$$

$$EA = E^0(A^- / A) - \Delta G_{sol} + const \tag{2.24}$$

$E^0_{(D^+/D)}$ is the oxidation potential of the donor and $E^0_{(A^-/A)}$ is the reduction potential of the acceptor measured in the same solvent. Combining equations (2.20) to (2.24) leads to the Rehm-Weller equation:

$$\Delta G^0_{SSIP} = E^0(D^+ / D) - E^0(A^- / A) - E_{00} + w_p - w_R \qquad (2.25)$$

The Rehm-Weller equation is used to calculate the free energy change of the PET reaction in solution from the redox potentials and the 0,0-energy, E_{00}. For the neutral reactants or only one reactant is uncharged, the work term, $w_R = 0$.

2.1.4. Marcus theory of electron transfer

2.1.4.1. Kinetics and rate expressions

After the absorption of light, there are various events taking place in excited acceptor (A*). The processes and their rate constants are depicted in Figure 2. 4.

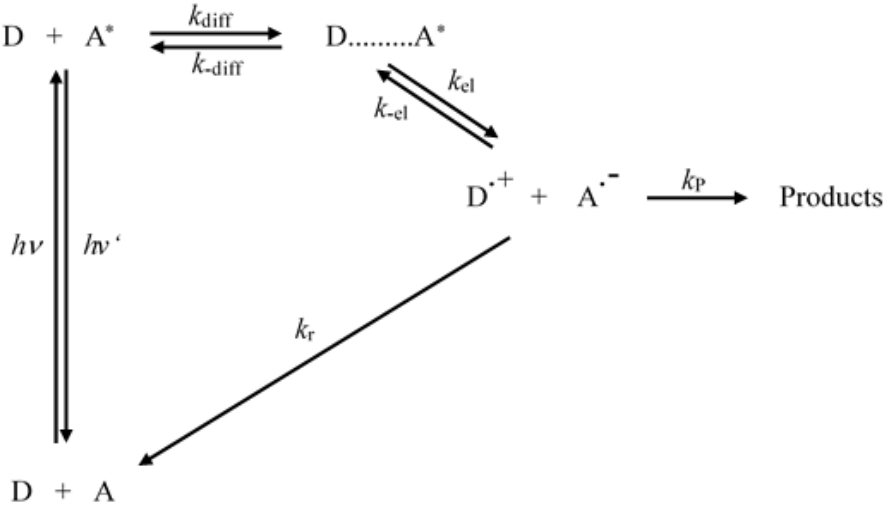

Figure 2.4. The various processes take place in the excited acceptor following excitation: k_{diff} and k_{-diff} are the diffusion controlled rate constants of the formation and dissociation of an encounter complex, respectively. k_{el} denotes the rate constant of the electron transfer in the encounter complex, k_{-el} gives the rate constant for the reverse electron transfer. k_r refers to the rate constant for the return electron transfer to ground-state reactants. k_p is the dissociation rate constant of the radical ions.

A steady-state treatment to the various steps in Figure 2.4 leads to the kinetic expression of the rate constant in bimolecular quenching reaction, k_q [44].

$$k_q = \frac{k_{diff}}{1 + \frac{k_{-diff}}{k_{el}} + \frac{k_{-diff} k_{-el}}{(k_p + k_r) k_{el}}} \tag{2.26}$$

With an assumption that $k_{el} >> k_{-el}$, the equation (2.26) becomes:

$$k_q = \frac{k_{el} k_{diff}}{k_{el} + k_{diff}} \tag{2.27}$$

A further assumption that $k_{diff} = k_{-diff}$ leads to [46].

$$\frac{1}{k_q} = \frac{1}{k_{el}} + \frac{1}{k_{diff}} \tag{2.28}$$

From eq (2.28), under conditions of fast electron transfer, i.e., $k_{el} >> k_{diff}$, the rate of the quenching process is given by the diffusion rate constant of the reactants, $k_q = k_{diff}$ (diffusion-controlled). Under slow electron transfer conditions, i.e., $k_{el} << k_{diff}$, electron transfer is activation-controlled. In this case, k_{el} can be determined from k_q, which measured by using Stern-Volmer method, and k_{diff} can be calculated using eq. (2.14) [47].

The rate of activation controlled electron transfer, k_{el}, can be expressed as a product of electron and nuclear factors:

$$k_{el} = \nu \kappa_{el} \kappa_n \tag{2.29}$$

Here, ν is the nuclear frequency factor and in a range from 10^{12} to 10^{14} s^{-1}. κ_{el} and κ_n refer to electronic and nuclear factors, respectively.

2.1.4.2. Activation and reorganization energy

Prior to electron transfer, the precursor complex (A…D) and the solvent molecules surrounding undergo structural rearrangements. The free energy change and the energy associated with the rearrangements determine the activation energy for electron transfer step. This relation is described by the classical Marcus equation [48].

$$\Delta G^{*} = \frac{(\Delta G^{0} + \lambda)}{4\lambda} \tag{2.30}$$

With $\lambda = \lambda_i + \lambda_O$

Here, λ_i denotes the inner reorganization energy (the energy change of bond lengths in reactants), λ_s is the outer reorganization energy (the energy change of the solvent molecules).

$$\lambda_i = \sum_i \frac{f_i^R f_i^P}{f_i^R + f_i^P} \Delta q_i^2 \tag{2.31}$$

Where f_i^R is the i^{th} force constant for the reactants and f_i^P being that for the products, Δq_i is the difference in the equilibrium bond distance between the reactant and product states corresponding to an i^{th} bond.

For two spherical reactants surrounded by the solvent molecules, λ_o can be expressed by:

$$\lambda_o = \frac{\Delta e_0^2}{4\pi\varepsilon_0}\left(\frac{1}{2r_A} + \frac{1}{2r_D} - \frac{1}{d_{cc}}\right)\left(\frac{1}{n^2} - \frac{1}{\varepsilon_s}\right) \tag{2.32}$$

Where Δe is the charge transferred in the reaction, r_D and r_A are the radii of the donor and the acceptor, respectively and d_{cc} is the center-to-center distance between the donor and acceptor. n and ε_s are the refractive index and dielectric constant, respectively.

According to the classical theories of electron transfer κ_n is expressed as:

$$\kappa_n = \exp(-\Delta G^{*} / RT) \tag{2.33}$$

Introducing eq. (2.33) in eq. (2.29) yields

$$k_{el} = \nu \kappa_{el} \exp(-\Delta G^{*} / RT) \tag{2.34}$$

In the classical approach by Marcus, κ_{el} is assumed to be unity (i.e., electronic barriers are neglected) and ΔG^{*} is considered as a function of the nuclear reorganization energy (λ) and free energy (ΔG^0) of the reaction. According to the non-classical or quantum mechanical approach, the overlap of the nuclear and electronic wave functions of the initial reactant and

final product states are used to evaluate these factors. Introducing eq. (2.30) in eq. (2.34) yields the Marcus equation for electron transfer rate constant.

$$k_{el} = \nu \exp\left[\frac{-(\lambda + \Delta G^0)^2}{4\lambda RT}\right] \tag{2.35}$$

In PET, the crossing point can be regarded as a transient photo-excited complex having a geometry just between the geometries of the reactant and product states. The activation energy consists of solvent and bond contributions and the Marcus treatment can be applied to calculate the energy barriers and rate constants.

2.1.4.3. Inverted region

According to the eq. (2.35), the plot of lnk_{et} vs ΔG^0 will be bell shaped (Figure 2.5).

If $-\Delta G^0 = \lambda$: The ET rate reaches a maximum value (Figure 2.6a).

If $-\Delta G^0 < \lambda$: The ET rate increases with larger driving force. This is called Marcus normal region (Figure 2.6b).

If $-\Delta G^0 > \lambda$: The ET rate decreases with larger driving force. This is called Marcus inverted region (Figure 2.6c).

Experimental evidence for the Marcus inverted region has been an elusive task. Weller, for example, has observed that the quenching rate constants for series of systems plateau at large driving force values [36, 44]. This behaviour is typical of fluorescence quenching experiments in solution and is termed as the Rehm-Weller behaviour. The lack of the observation in the Marcus inverted region has been suggested [49]:

- Perhaps more than one mechanism may be involved in the quenching mechanism, for example, the formation of an excited-state (an exciplex), would proceed faster than the formation of the radical ion pairs.
- The inverted region can be obscured in bimolecular ET by diffusion kinetics [37]. The actual rates of the ET are rapid than the rates of diffusion encounters. In Weller's work, the rates of quenching are measured when what is really wanted are the rates of ET. If the latter are more rapid than the rates of diffusion and then the actual rates of ET can be obscured.
- Or for back ET reaction

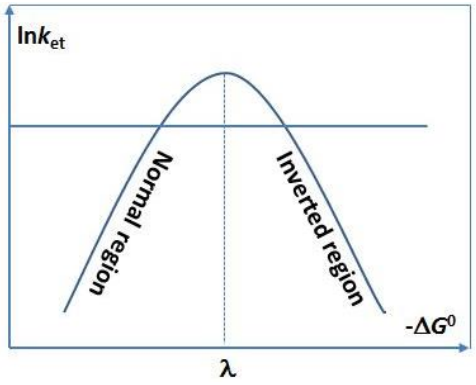

Figure 2.5. The variation of lnk_{et} vs driving force (-ΔG^0) of the electron transfer reaction.

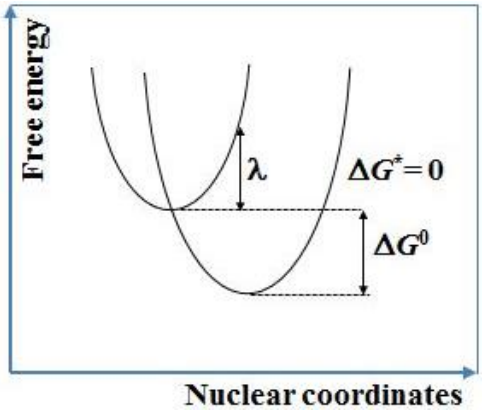

(a) Activationless region

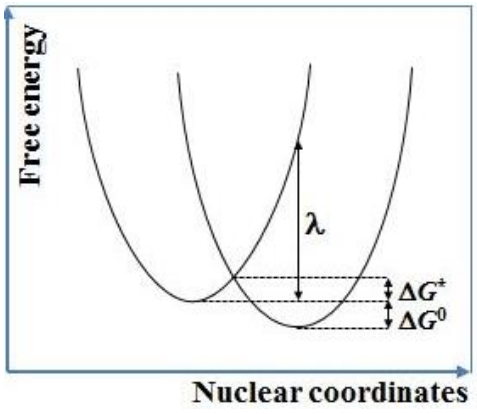

(b) Normal region

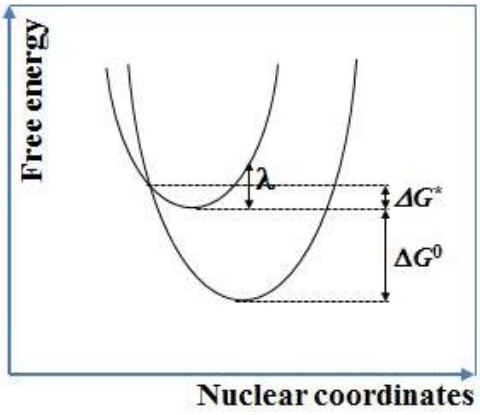

(c) Inverted region

Figure 2.6. The free energy surfaces of the reactant and product in different regions in the Marcus theory of the electron transfer.

2.2. Quantum mechanical treatment of spin evolution and magnetic field effect

2.2.1. Spin magnetic moment

According to quantum mechanics, the electron has its own angular momentum, which is independent of the angular momentum. This independent angular momentum is called spin. For an electron, the magnetic moment (μ_s) due to its spin (S) is given by:

$$\mu_s = -g\mu_B S \tag{2.36}$$

Here, g is called the g-factor, which is 2 for the spin magnetic moment of a free electron, μ_B is the Bohr magneton.

The operators for the electron spin angular momentum obey the following relations.

$$S^2 \left| S, m_S \right\rangle = S(S+1) \left| S, m_S \right\rangle \tag{2.37}$$

$$S_z \left| S, m_S \right\rangle = m_S \left| S, m_S \right\rangle \tag{2.38}$$

Here, S is the spin quantum number and m_S the magnetic quantum number of electron spin. For a single electron, $S = 1/2$ and m_S = ±1/2. S_z is the z-component of the electron spin operator.

2.2.2. Spin in magnetic field

In the absence of a magnetic field, the spin (magnetic) substates represented by the quantum number m_S = ±1/2 are degenerate. By applying an external magnetic field (z-axis), the magnetic moment interacts with the field, the degeneracy is lifted, the spin substates adopt now two orientations with respect to the field along the z-axis:

- α - state (parallel spin state): m_S = +1/2, spin up with the energy is given by:

$$\text{E } (+1/2) = +1/2 g\mu_B B \tag{2.39}$$

Where B is applied magnetic field strength.

- β-state (antiparallel spin state): m_S = -1/2, spin down with the energy given by:

$$\text{E } (+1/2) = +1/2 g\mu_B B \tag{2.40}$$

This interaction of the electron spin with the applied magnetic field results in an energy difference between the parallel and antiparallel spin-states given as:

$$\Delta E = g\mu_B B \tag{2.41}$$

However there are further pattern of splitting of these energy levels due to hyperfine interaction with the neighboring nuclei. The following Figure 2.7 shows the alignment of the spin with respect to the magnetic field along *z*-axis.

2.2.3. Vectorial representation of radical ion pairs

The possible orientations of two electron spins in radical ion pair (RIP) can exist in a singlet state, the spin vector on the electron 1 is aligned in α–state (m_{S1} = +1/2) while that on the electron 2 is aligned in β–state (m_{S2} = -1/2), $M_S = m_{S1} + m_{S2} = 0$. An alternative triplet state can be formed from the two spins, with three substates. The possible orientation include a) with both electron spins aligned parallel to the field, (M_S = 1) and termed as the $T_+(\alpha\alpha)$ state; b) both aligned anti-parallel (M_S = -1) termed as the $T_-(\beta\beta)$ state; c) one spin parallel (α) and one spin anti-parallel (β) with M_S =0 along the field axis (but the spins are not 180^0 out of phase) and termed as the $T_0(\alpha\beta)$ state. The states are pictorially represented in Figure 2.8.

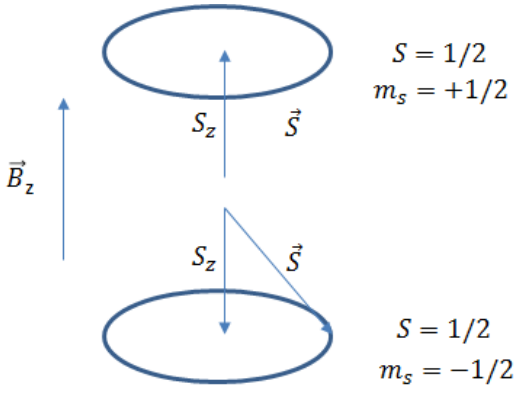

Figure 2.7. The possible orientations of two electron spins under the effect of an applied magnetic field.

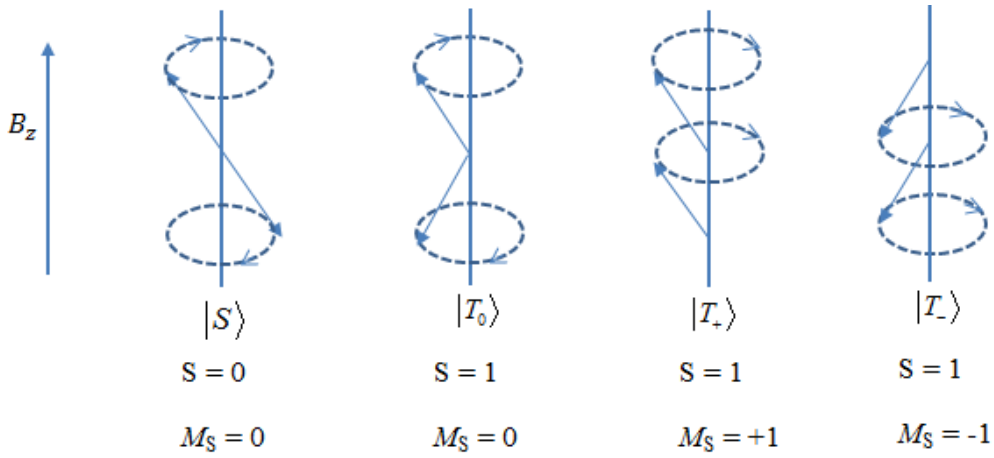

Figure 2.8. Vector model of the spin states of RIP. S denotes overall spin quantum number. While the singlet remains with the two spin 180^0 out of phase, the triplet states are with their spins aligned mutually in three ways to match their M_S = +1, 0, -1 values.

2.2.4. Wave-function of the RIP Spin states

The combination of two electron spins (S_1 and S_2, S_1=S_2 = 1/2) in RIP yields the singlet ($|S\rangle$) and three triplet ($|T_{\pm,0}\rangle$) states. They can be presented via the product of the electron and nuclear spin wavefunctions:

a) Singlet and triplet electron spin wavefunctions:

$$|S\rangle = (|\alpha_1\beta_2\rangle - |\beta_1\alpha_2\rangle)/\sqrt{2} \quad (2.42)$$

$$|T_0\rangle = (|\alpha_1\beta_2\rangle + |\beta_1\alpha_2\rangle)/\sqrt{2} \quad (2.43)$$

$$|T_{+1}\rangle = |\alpha_1\alpha_2\rangle \quad (2.44)$$

$$|T_{-1}\rangle = |\beta_1\beta_2\rangle \quad (2.45)$$

b) The nuclear spin wavefunctions is presented as follows:

$$|\chi_N\rangle \prod_i^a |m_{I,i}\rangle \prod_j^b |m_{I,j}\rangle = |m_{I,i}, m_{I,j}\rangle \quad (2.46)$$

Where $m_{I,i}$ and $m_{I,j}$ denote the magnetic spin quantum numbers on atom *i* of the radical 1 and atom *j* of radical 2, respectively.

For simplicity, we can write

$$|\chi_N\rangle = \prod_i^a M_i \rangle \prod_k^b M_k \quad (2.47)$$

Or $$|\chi_N\rangle = |M_i M_k\rangle \quad (2.48)$$

In the absence of an external magnetic field, the energies of the singlet and triplet radical pairs can be presented as follows.

$$E(S) = \left\langle S \left| H_{ex} \right| S \right\rangle = J \tag{2.49}$$

$$E(T_n) = \left\langle T_n \left| H_{ex} \right| T_n \right\rangle = -J \tag{2.50}$$

2.2.5. The RIP Spin Hamiltonian

A RIP consists of two weakly coupled radicals and its total Hamiltonian comprises of the magnetic and the exchange terms.

$$H_{RP} = H_{ex} + H_{mag} \tag{2.51}$$

$$\text{Where } H_{ex} = -J\left(2S_1S_2 + 1/2\right) \tag{2.52}$$

With J is the exchange interaction between two electron spins S_1 and S_2.

$$H_{mag} = \underbrace{(g_a\mu_B S_{1z}B + \sum_i^a A_i S_1 \hat{I}_i)}_{Radical1} + \underbrace{(g_b\mu_B S_{2z}B + \sum_k^b A_k S_2 \hat{I}_k)}_{Radical2} \tag{2.53}$$

The first and second terms in eq. (2.53) refer to Zeeman and hyperfine interactions of the component radicals. g_a and g_b are g-values of the radical a and b, respectively, and A_i and A_k are isotropic hyperfine coupling constants with nuclear spins I_i and I_k in radicals a and b.

The quantum mechanical exchange interaction is described as the overlap of the electronic wavefunctions of two unpaired electrons and their spins exchange. J(r) depends on the separation distance, r, between two radicals.

$$J(r) = 2\int \psi_1^*(r_1)\psi_2^*(r_2)\tfrac{1}{|r_1 - r_2|}\psi_2(r_1)\psi_1(r_2)d_{r1}d_{r2} \tag{2.54}$$

Where $\psi_i(r_j)$ represents the wavefunction of electron i at position r_j. Experiment has proven that the exchange interaction decreases exponentially with separation distance [50].

$$J(r) = J_0\exp(-\xi r) \tag{2.55}$$

When the inter-radical distance increases in the order tens of angstroms, the exchange interaction falls off to zero. When J(r) is negative, the distance dependence of the energies of the singlet and three triplet states in the absence and presence an external magnetic field is shown in Figure 2.9. The energy of the singlet state is lower than that of the three triplet states

and their energy gap decreases with increasing the inter-radical distance. In the absence of an external magnetic field, when the distance between two radicals is large enough, the S and $T_{\pm,0}$ states become degenerated (region I in Figure 2.9a).

In the presence of the field, due to Zeeman interaction, S-T_0 conversion occurs at region I and S-T- are crossed at a level-crossing distance $r = r_{LC}$ (Figure 2.9b).

The singlet and triplet energies in the presence of an external magnetic field are expressed as follows:

$$E(S) = \left\langle S \left| H_{ex} + H_{mag} \right| S \right\rangle = J \tag{2.56}$$

$$E(T_n) = \left\langle T_n \left| H_{ex} + H_{mag} \right| T_n \right\rangle = -J + ng\mu_B B + \frac{n}{2}\left(\sum_i^a A_i M_i + \sum_k^b A_k M_k \right) \tag{2.57}$$

Here n = -1, 0, +1 and $g = (g_a + g_b)/2$

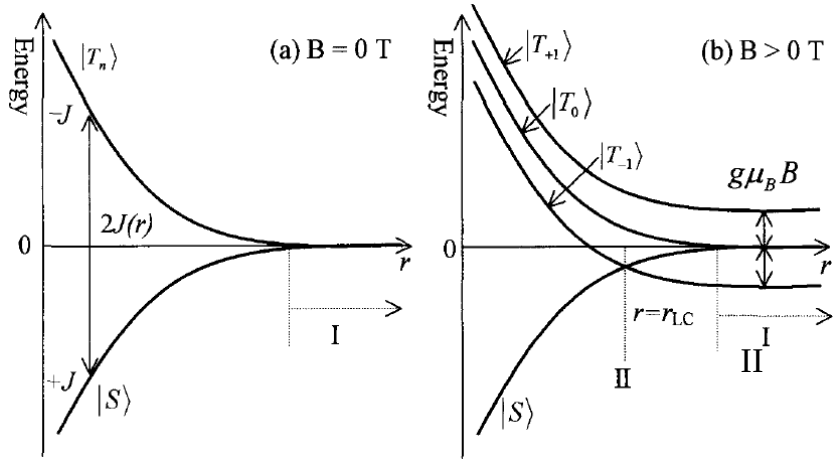

Figure 2.9. The inter-radical separation (*r*) dependence of the singlet and triplet radical ion pair energies in the absence (a) and presence (b) of an external magnetic field effect. *J*(r) is negative. r_{LC} refers to the level-crossing distance. The regions are described as I and II.

2.3. Classification of magnetic field effects due to radical pair mechanism

As mentioned above, when the energy gap between $|S\rangle$ and $|T_{\pm,0}\rangle$ is degenerated, S-T conversion occurs through the following off-diagonal matrix elements:

$$\left\langle T_0, \chi_N \left| H_{ex} + H_{mag} \right| S, \chi_N \right\rangle = 1/2\left[\Delta g \mu_B B + \left(\sum_i^a A_i M_i - \sum_k^b A_k M_k \right) \right] \tag{2.58}$$

$$\left\langle T_{\pm 1}, \chi_N^{'} \left| H_{ex} + H_{mag} \right| S, \chi_N \right\rangle = \frac{\mp A_i}{2\sqrt{2}} \left[I_i(I_i+1) - M_i(M_i \mp 1) \right]^{1/2} \tag{2.59}$$

Here $\Delta g = g_a - g_b$; $\left|\chi_N^{'}\right\rangle = \left|M_i^{'}, M_k^{1}\right\rangle$; $M_i^{'} = M_i \mp 1$; $\left|\chi_N\right\rangle = \left|M_i, M_k\right\rangle$; $M_k^{'} = M_k$

The S-T conversion can be obtained:

(a) $\left|S\right\rangle - \left|T_{\pm,0}\right\rangle$ conversion occurs through the HFC term in eqs. (2.58) and (2.59) at large inter-radical separation in the absence of an external magnetic field.

(b) $\left|S\right\rangle - \left|T_0\right\rangle$ conversion occurs through eq. (2.58) in the presence of an external magnetic field at large *r* value.

(c) When *J*(r) is negative, $\left|S\right\rangle - \left|T_{-1}\right\rangle$ conversion occurs through HFC term in eq. (2.59) at $r = r_{LC}$ (Figure 2.9).

Thus, the MFEs on chemical reactions through radical ion pairs can be classified by the following mechanisms:

(1) The Δg mechanism: This mechanism is applicable when $J = 0$; $\Delta g \neq 0$; and $A_i = A_k = 0$.

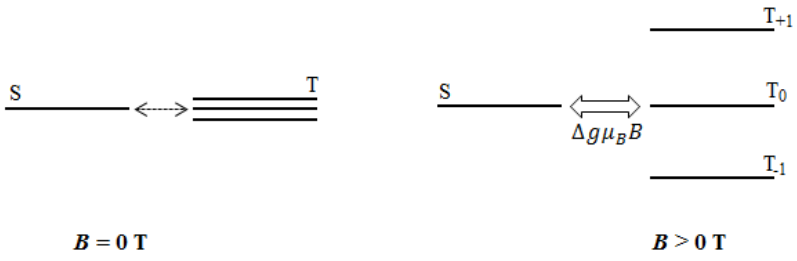

Figure 2.10. The effect of an external magnetic field on singlet-triplet conversion in the Δ*g* mechanism.

In the absence a magnetic field, S-T conversion is impossible. However, S-T_0 conversion occurs in the presence of a magnetic field through the Δ*gB* term in eq. (2.58).

(2) The hyperfine coupling mechanism: This mechanism is applicable when $J = 0$; $\Delta g = 0$; $A_i \neq 0$; and/or $A_k \neq 0$.

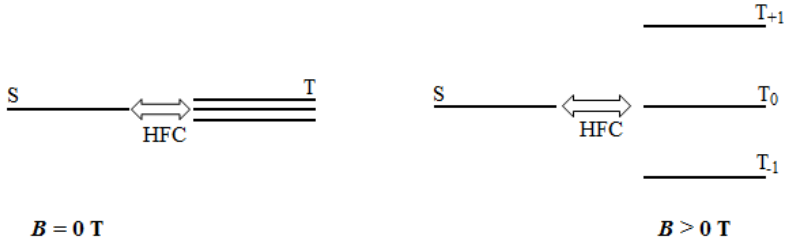

Figure 2.11. The effect of an external magnetic field on singlet-triplet conversion in the hyperfine coupling mechanism.

S-$T_{\pm,0}$ conversion is possible at a zero field through the HFC terms in eqs. (2.58) and (2.59). By applying a magnetic field, due to Zeeman interaction, $T_{\pm}$ states are lifted. There is only S-T_0 conversion through the HFC term in eq. (2.58).

(3) The level-crossing mechanism: This mechanism is applicable when $J \neq 0$; $A_i \neq 0$; and/or $A_k \neq 0$.

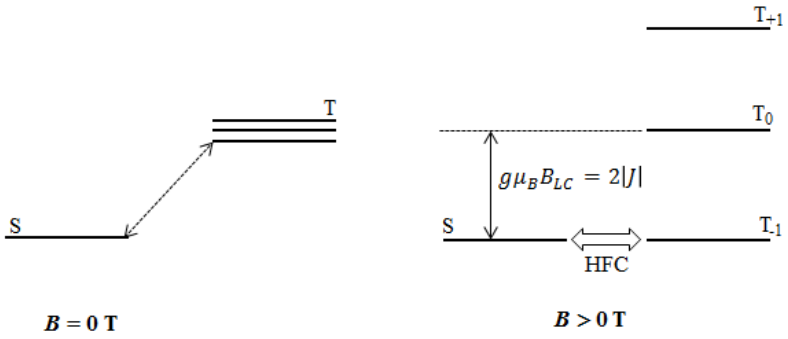

Figure 2.12. The effect of an external magnetic field on singlet-triplet conversion in the level-crossing mechanism.

There is no S-$T_{\pm,0}$ conversion in the absence of a magnetic field due to the energy difference ($2|J|$) between singlet and triplet states. At $B = B_{LC}$ T, the level-crossing occurs between singlet and T_- states through the HFC term in eq. (2.59).

2.4. Magnetic field effects on the exciplex fluorescence

If the fluorescence intensity of an excited complex (exciplex) is sensitive to the presence of an external magnetic field, the phenomenon is said to show a magnetic field effect on the exciplex. Exciplex fluorescence in the studied systems in this work is magnetosensitive. The origin of this effect will be illustrated below.

2.4.1. The photo-induced electron transfer reaction scheme and time-resolved magnetic field effects of the exciplexes

Exciplexes appear as intermediates in intra- and inter-molecular photo-induced ET in solution [51-54]. In general, exciplexes can be observed by their emission, which is, in the most favourable cases, spectrally well separated from the locally excited fluorescence [55-57].

Furthermore, under suitable conditions, this exciplex emission is sensitive to an external magnetic field [1, 4-7, 13-20]. MFEs on exciplexes result from the inter-conversion of the singlet and the three triplet states of the radical ion pair (RIP) in equilibrium with the exciplex. The presence of an external magnetic field lifts the degeneracy of the three triplet states and thus, reduces the rates of singlet-triplet conversion ($S\text{-}T_{\pm}$), which in these systems is induced by the hyperfine interaction [21-23, 58]. This causes an increase of the population of the initial spin state in the presence of an external magnetic field. Due to the reversible conversion of the exciplex and the singlet RIP, the exciplex luminescence becomes magnetosensitive.

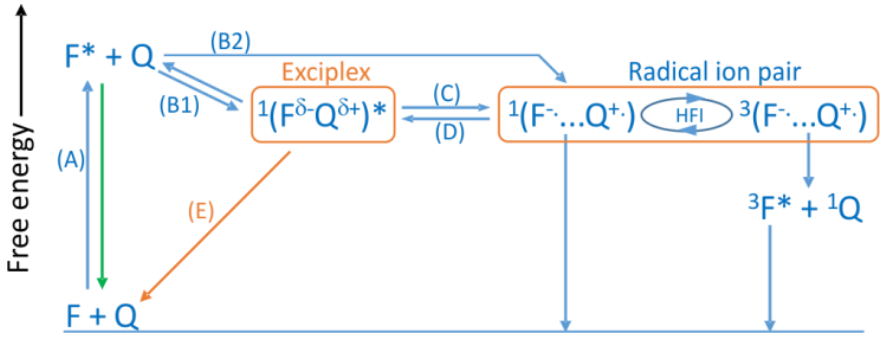

Scheme 2.1. The possible reaction pathways and species involved in the magnetic field effect of the exciplex: Photo-excitation (A), exciplex formation (B1), direct formation of RIP via distant ET (B2), exciplex dissociation into RIP (C), singlet-triplet conversion by hyperfine interaction (HFI), RIP re-forms into exciplex (D) and exciplex luminescence (E). The abscissa is a projection of two-dimensional reaction ordinate including the inter-particle distance and outer-sphere ET ordinate-solvent rearrangement. The orange and green arrows refer to the emissive processes of either the exciplex or the locally excited fluorophore. The former is detected in the experiment. F and Q denote fluorophore and quencher, respectively. Spin multiplicities are indicated by superscripts.

Scheme 2.1 depicts a reaction scheme of the photo-induced ET processes of an exciplex-forming fluorophore-quencher system. The involved species can be classified by their inter-particle distance and the solvent polarization expressed by the Marcus outer-sphere ET coordinate. Here, the horizontal arrangement is arbitrary. The observation of the magnetic field effect on exciplexes is preceded by the formation of the singlet RIP, which can be formed via distant ET (B2; capital letters are referring to reactions in Scheme 2.1) or by the

dissociation of an exciplex (C) formed via reaction (B1). Note, that the singlet and triplet RIPs can undergo charge recombination, yielding the ground state and the fluorophore triplet state, respectively. The singlet back ET to the ground state is typically located in the Marcus inverted region and, hence, is slow [59-61]. Furthermore, since the exciplex dissociation is typically a slow process, the ions resulting from exciplex dissociation will be delayed with respect to the loose ions formed by direct electron transfer. As a consequence the MFE generated by the exciplex route will also be delayed (to be discussed in Results and Discussion part). Thus, time-resolved studies of MFE of the exciplexes, allows deducing of the initial quenching state (i.e., B1 vs B2 in scheme 2.1). This methodology has been introduced in ref. 20 and the interested reader is referred to this work for additional details.

2.4.2. The influence of the solvent on the magnetic field effects of the exciplexes

The diffusional motion of radicals and spin evolution of RIP play an important role in the magnitude of the MFE of the exciplex. The solvent environment can control these two factors. As mentioned above, the spin evolution can only take place if two radicals in RIP can diffusively separates until the exchange interaction has decayed considerably. The inter-radical distance can be controlled by the solvent polarity (dielectric constant, ε_s) and the viscosity (η).

If the solvent polarity is low, the component radicals cannot separate to the region where spin evolution occurs. Thus, MFEs is low. If the polarity is high, the inter-radical separation is sufficient but the reencounter probability of two radicals in geminate cage is ineffective. As a consequence MFE is small. In order to obtain the maximum MFE values, the solvent polarity is chosen to attain a good compromise between separation distance and reencounter probability.

2.4.2.1. Binary solvent mixtures and magnetic field effect

The effect of the solvent parameters on the MFE of the exciplex has generally been discussed. The origin of the modification of the MFE magnitude results from the change of the RIP dynamics by the solvent molecules surrounding RIP. The solvent molecules create a solvent shell, especially in solvent mixtures. The presence of polar components in the mixture around the RIP plays a crucial role in the geminate reaction. The new interesting starts appearing. The polar solvent molecules surround the solutes (RIPs) by non-covalent bonds. This process is

known as solvation. The preferential solvation or the enrichment of the polar components in mixture giving rise to the micro-composition around the solute is not as the bulk composition. This effects on the RIP dynamics what is reflected on the MFE of the exciplex. In particular, when the dielectric constants of two components in the binary solvent mixture differ widely, e.g. toluene (ε_s = 2.4)/dimethylsulfoxide (ε_s = 50.0) mixture, forming a micro-heterogeneous binary solvent, the effect is more sufficient.

2.4.2.2. Binary solvent mixtures: Models

A model to theorize and quantify the effect of the dielectric enrichment in binary solvent mixture is a challenge. The aim of each model is to provide a physical picture of the interactions of the solvent molecules and the solutes in solution.

The useful information of this aspect has been done by Suppan [62] who investigated the solvatochromic shifts in binary solvents and concluded that the cluster of polar components (polar micro-domains) around the solutes is formed via the preferential dielectric interaction of the solute intermediates with the polar components in the binary mixture, something resulting from the effect of the increased solvent stabilization energy as a result of dipole-dipole forces which increase with increasing polarity. According to this model, the dimension of the polar micro-domains is the characteristic length of the ion-dipole interaction, i.e. where $e_0\vec{u}/\varepsilon_s \approx k_B T$, where e_0 is the electron charge, $\vec{u}$ is the dipole moment, ε_s is the relative permittivity, k_B is the Boltzmann constant and T is the absolute temperature. Under the conditions of thermodynamic equilibrium, when this increase in stabilization energy is compensated by the loss in entropy of mixing, one can show that the index of preferential solvation is related to the molar ratio of the components (nonpolar and polar components) in bulk $\left(X = x_{N,bulk}/x_{P,bulk}\right)$ and the molar ratio of the components in the solvation shell $\left(Y = y_{N,solvation}/y_{P,solvation}\right)$ by the following relation:

$$Y = Xe^{-Z} \tag{2.60}$$

Where Z is the 'index of preferential solvation' given by:

$$Z = CM\mu_M^2 \Delta f(D)_{N,P}/2\delta Ra^6 \tag{2.61}$$

Where M and δ are the solvent mean molecular weight and density, respectively. $\Delta f(D)_{N,P} = f(D)_P - f(D)_N$, μ_M is the solute molecules dipole moment, R is the gas constant and a is the molecular radius. C is a constant. However, Suppan's model could not explain some of the effects of MFE observed.

The model is based on the concentration fluctuation [3]. It can be described by:

$$(\Delta x_P)^2 = RT/(\partial \mu_P/\partial x_P)_{V,T} \tag{2.62}$$

Where x_P is the mole fraction of the polar component of the binary mixture, $(\Delta x_P)^2$ is its concentration fluctuation in a certain given volume, R is the gas constant and μ_P is the chemical potential of the polar component.

According to the Hildebrandt theory [63, 64], the chemical potential of the polar component is given by:

$$\mu_P \approx \mu^0 + RTlnx_P + \phi_N^2 V_{mP}(\delta_P - \delta_N)^2 \tag{2.63}$$

Here $\phi_N = [1 + (V_{mP}/V_{mN})x_P]^{-1}$, δ is the empirical parameter of solubility given as $\delta = \sqrt{E/V_m}$, where E is the molar energy of cohesion and V_m is the molar volume playing an important role in the Hildebrandt theory. Substituting all these expressions in eq. (2.62) yields

$$(\Delta x_P)^2 \approx \frac{x_P}{1-2V_{mP}(\delta_P-\delta_N)^2\frac{x_P}{RT}} \tag{2.64}$$

when $2V_{mP}(\delta_P - \delta_N)^2 \to 0$, leads to $(\Delta x_P)^2 = x_P$, a condition when fluctuations are not perceptible. But when the above parameter tends to unity, the value of $(\Delta x_P)^2$ may exceed statistical levels of a perfect mixture.

A dielectric continuum model of the micro-heterogeneous solvation in binary mixtures has been recently described by Basilevsky et al [65]. This model can be generalized for the case of RIPs [6]. According to this model, the solvation parameters such as the dielectric constant, ε_s(r), the local concentration of the polar component (dimensionless local concentration) , y(r) are space-dependent and they are the important variables controlling the solution properties. Furthermore the potential of mean force (PMF) has been expressed and calculated as well. It, thus, replaces the simpler forms [3, 66-68].

We consider a solvent mixture composing of toluene (TOL) and dimethylsulfoxide (DMSO) as non-polar and polar solvent components. c_1, c_2 and c are local concentrations of TO, DMSO, and the total concentration ($c = c_1 + c_2$). The $<c_1>$, $<c_2>$, and $<c>$ ($<c> = <c_1> + <c_2>$) are average concentrations. The dimensionless concentrations are given as:

$y = \frac{c_1}{c_2}$ and $z = \frac{c}{\langle c \rangle}$. The y and z values are continuous functions of a space point, r.

The total average concentration or the total density, z(r) obeys Morse function:

$$z(r) = 1 + \exp\left[-2\alpha(r_{\min} - a)\right] - 2\exp\left[-\alpha(r_{\min} - a)\right] \tag{2.65}$$

Where, α is an adjustable parameter, a is the Born ion radius and $r_{\min}$ refers to the scalar distance to the closest ion. The dielectric permittivity ε(r) depending on dimensionless local concentrations y(r) (DMSO) and total density, z(r), is given by:

$$\varepsilon(r) = 1 + 4\pi\chi_\infty z(r) + 4\pi\chi y(r) z(r) \phi(z(r)) \tag{2.66}$$

Here, χ_∞ and χ are inertialess (fast electronic) and inertial (slow, nuclear, associated with permanent charge distributions of DMSO particles) components of the solvent susceptibility and ϕ(z) = exp[(z-1)/z_0], with an adjustable parameter z_0.The electrostatic part of the solvation free energy, in terms of the varying local concentration y(r) and density z(r), is calculated over the total external volume [69]:

$$G_{el} = -\frac{1}{2}\int_a^\infty r^2 dr \left(1 - \frac{1}{\varepsilon(r)}\right)\left(\frac{Q}{r^2}\right)^2 \tag{2.67}$$

Here, a and Q refers to the ion radius and charge. The mixing of the two components results in the entropic changes, an equilibrium condition for y(r) is found:

$$\ln\frac{y(r)}{1 - y(r)} = \ln\frac{y_\infty}{1 - y_\infty} + \frac{F(r)}{k_B T \langle c \rangle}\phi(z(r)) \tag{2.68}$$

$$\text{With } F(r) = \frac{\chi}{2\left[\varepsilon(r)\right]^2}\left(\frac{Q}{r^2}\right)^2 \tag{2.69}$$

y_∞ corresponds to the asymptotic value $y(r \to \infty)$. The solution of equations (2.68) and (2.69) gives y(r) and ε(r).

The potential of mean force (PMF) can be calculated by:

$$W(L) = -\frac{Q^2}{L} - \frac{C_6}{L^6} + \frac{C_{12}}{L^{12}} + W_{solv}(L) \tag{2.70}$$

With L being the inter-radical separation. The first three terms refers to the vacuum interaction (the Coulomb attraction and Lennard-Jones (LJ) contributions with C_6 and C_{12} being the LJ coefficients and $Q = \pm 1$. The last term, denoting the electrostatic solvation effect, is defined by:

$$W_{solv}(L) = G_{el}(L) - G_{el}(L = \infty) \tag{2.71}$$

2.5. The principle of single photon counting and the time-resolved mode

In the time-resolved mode, the sample is excited by a suitable pulsed light source and the decay intensity of the compound under investigation is recorded. If an external magnetic field is applied in the experimental condition, the influence of a magnetic field on the lifetime of the excited states in sample can be studied.

Time-Correlated Single Photon Counting (TCSPC), also referred to as Single Photon Timing (SPT) is a commonly used technique for the determination of excited state lifetimes [70]. After the sample is excited by a light pulse, the molecules in the excited state decay exponentially. (Figure 2.13). In order to measure this decay, the apparatus is adjusted in a way, so that, at maximum, only one photon per light pulse is collected. In the following, the time span between the light pulse and the arrival of the photon on the detector is recorded. This procedure has to be repeated a large number of times.

A Multi Channel Analyser (MCA) then sorts the incoming photons according to the elapsed time between the light pulse and the detector signal. Whereby the total time is divided into different time intervals (channels) and the number of photon events per time interval is counted. As the exact time of photon emission after excitation of a molecule is solely determined by statistic, the recording and summing up of counts in the different time intervals of the MCA exactly correlates with the decay curve of the molecule under investigation. When collecting the data from a statistically representative number of light pulses, one should thus be able to extract the lifetime of the molecule by analyzing the recorded decay curve.

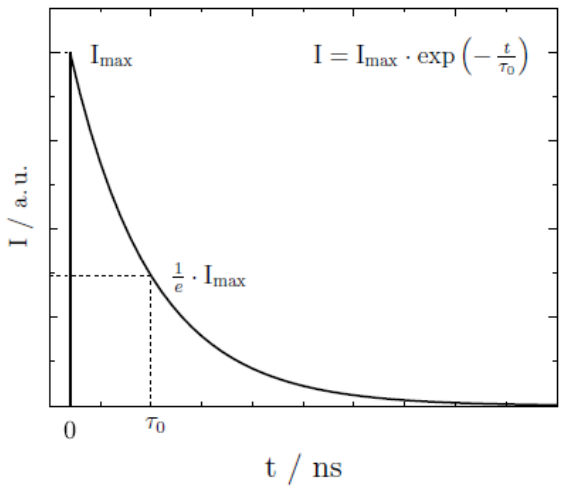

Figure 2.13. The excited states decay exponentially in TCSPC measurement. The lifetime is defined as the time at which the intensity decreases to 1/*e* of the intensity at $t = 0$ (I_{max}).

3. EXPERIMENTAL

3.1. Simulations

Simulation model:

In this work a model in which the initial quenching products and the reversible conversion of the singlet RIP and the exciplex taken into account was used to simulate the time-resolved MFE data (Figure 3.1). The probability of the exciplex state, ρ_E, in this model is given by [20]:

$$\rho_E(t, B_0) = \phi_E + \phi_I R(t|r_I, B_0) + k_d \int_0^t \rho_E(\tau) R(t-\tau|r_E, B_0) d\tau - (k_d + \tau_E^{-1}) \int_0^t \rho_E(\tau) d\tau \quad (3.1)$$

The first term in equation (3.1) refers to the probability of the initial exciplex formation (pathway B1 in Scheme 1), ϕ_E = 1- ϕ_I. The second contribution is the probability of the initial singlet RIP formation (pathway B2 in Scheme 1), ϕ_I, and its recombination into the exciplex until *t*, $R(t|r_I, B_0)$. r_I is the distance where the singlet RIP is formed via distant ET. The third term denotes the probability that the exciplex is reformed until *t*, $R(t-\tau|r_E, B_0)$ and dissociates with the probability $k_d \rho_E dt$ at τ. r_E and k_d give the distance where the exciplex is formed and the exciplex dissociation rate constant (Figure 4.6), respectively. τ_E is the exciplex lifetime (Figure 4.7).

The association constant, $K_a = k_a/k_d$ (k_a is the rate constant of the exciplex formation from the RIP association), has been determined (besides ϕ_I and ϕ_d) by extracting from the experimental MFE data by least-squares fitting. The K_a-values so obtained are plotted in Figure 4.8 as a function of static dielectric constant, ε_s.

Simulation parameters:

The time-resolved magnetic field effect depends on the following parameters:

- Diffusive motion: D, r_E, r_c, hydrodynamic hindrance.
- Exciplex: τ_E, $\phi_d = k_d \tau_E$
- RIP: Spin evolution, τ_R, r_I, ϕ_I, $k_a = K_a k_d$

Most of listed parameters are either known, or can be determined experimentally and kept constant during the simulations:

Diffusion coefficient (D = 220 Å^2/ns) is estimated from the Stokes-Einstein relation assuming a hydrodynamic radius of 3.25 Å; r_E is 6.5 Å; r_c denotes the Onsager radius ($r_c = \frac{e_0^2}{4\pi\varepsilon_0\varepsilon_s k_B T}$), calculated from ε_s. The Deutch-Felderhof model was used for the hydrodynamic hindrance [71]; τ_E can be determined experimentally by fitting to the initial exciplex decay, $\phi_d = k_d \tau_E$ gives the exciplex dissociation quantum yield (detailed formula formation can be found in appendix…), ϕ_d values obtained are closed to those calculated from the dependence of τ_E on ε_s.

Spin evolution can be calculated using the hyperfine coupling constants described in Table 3.1-2. The radical ion pair lifetime, τ_{RIP}, is 100 ns, r_I is 7 Å, ϕ_I denotes the initial probability of the single RIP state. $k_a = K_a k_d$ is the rate of the singlet RIP association into the exciplex, K_a is the association constant. K_a and ϕ_I are determined by fitting the experimental MFEs.

Table 3.1. Hyperfine coupling constants, a_{-}^{H}, for the 9,10-dimethylanthracene$^{-\cdot}$ radical anion, from [72].

Value / mT	0.388	0.290	-0.152
Type	6H	4H	4H
Position	(-2CH_3)	(1, 4, 5, 8)	(2, 3, 6, 7)

Table 3.2. Hyperfine coupling constants, a_{+}^{H}, for *N*,*N*-dimethylaniline$^{+\cdot}$ radical cation. No experimental values are available, the values below have been calculated using DFT (UB3LYB/EPRII).

Value / mT	0.833	-0,428	0.0868	-0.722	1.30
Type	1N	2H	2H	1H	6H
Position	(N)	(2, 6)	(3, 5)	(4)	(-2CH_3)

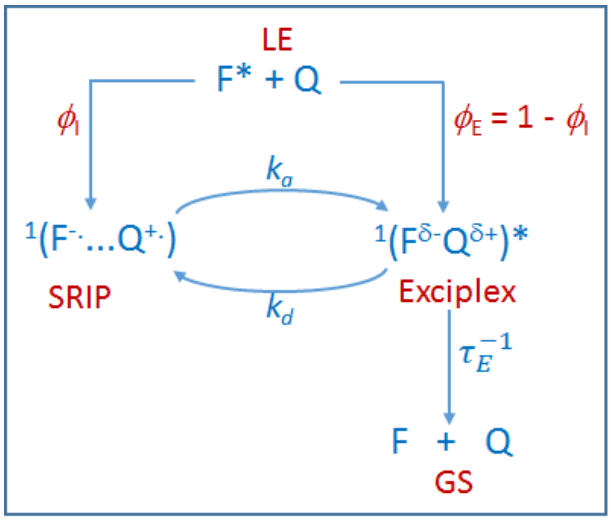

Figure 3.1. Graphic visualization of the exciplex kinetics of F/Q pair: ϕ_I gives the probability of the singlet radical ion pair (SRIP) is initially formed while $\phi_E = 1-\phi_I$ denotes the probability of the initial exciplex formation. The exciplex dissociates into the singlet radical ion pair with the rate constant, k_d, the SRIP associates into the exciplex with the rate constant, k_a and the radiative/non-radiative exciplex decay to the ground-state (GS) with the rate constant, τ_E^{-1}. LE gives to the locally-excited fluorophore.

Calculations of the Singlet Probability / and the Recombination Function: Details can be found appendix A3. For the pseudo first-order self-exchange rate constant, $k_{ex} = 1/\tau_{ex}$, a value of τ_{ex} = 8 ns was used in all simulations. Figure 3.2 gives the calculated singlet probability versus time for 9,10-dimethylanthracene/*N*,*N*-dimethylaniline.

3.2. Reactants

The fluorophore (F)/quencher (Q) pair selected for this investigation composes of electron acceptor 9,10-dimethylanthracene (DMAnt, Aldrich, 99%, used as received) and *N*,*N*-dimethylaniline (DMA, Aldrich, 99.5%) as electron donor. Quencher was distilled under reduced pressure and subsequently handled under an argon atmosphere. Physical parameters and chemical structures of the used fluorophore and quencher are given in Table 3.3 and Figure 3.3.

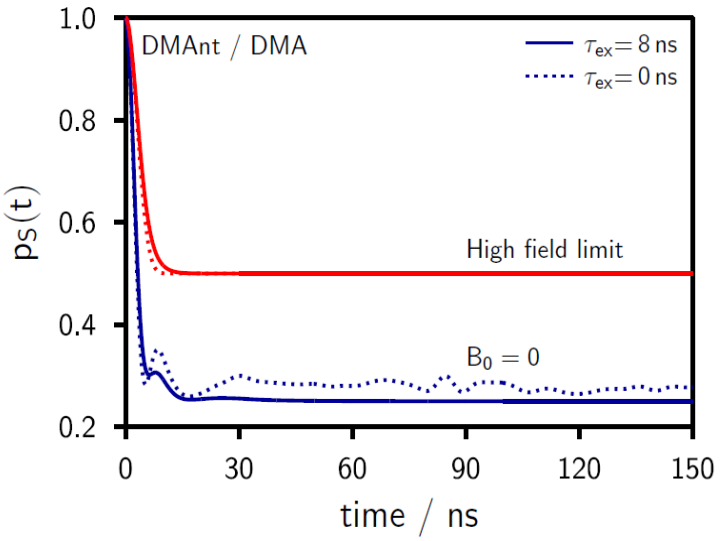

Figure 3.2. Singlet probability vs time for 9,10-dimethylanthracene/*N*,*N*-dimethylaniline was calculated at zero field and high field limit. The solid lines give $p_S(t)$ when the electron self-exchange taken into account with τ_{ex} = 8 ns, whereas the dash lines refer to $p_S(t)$ when the electron self-exchange neglected.

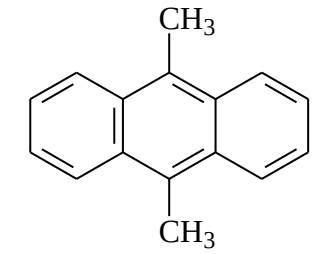

9,10-Dimethylanthracene
(DMAnt)

Fluorophore

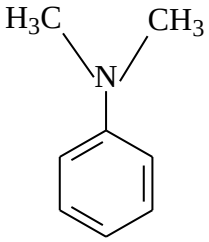

N,*N*-Dimethylaniline
(DMA)

Quencher

Figure 3.3. Chemical structures of fluorophore and quencher used in experiments.

3.3. Solvents

The solvent medium strongly affects on the magnetic field effect of the exciplex and the mechanism of the fluorescence quenching reactions, i.e., the initial quenching products (exciplexes and RIPs) [1, 20]. Therefore we have designed two binary solvents in terms of micro-homogeneity and micro-heterogeneity. The two solvent systems provide different micro-environments ranging from highly heterogeneous (toluene/dimethylsulfoxide) to

homogeneous (propyl acetate/butyronitrile) owing to difference in static dielectric constants of the constituting solvents (Table 3.4).

Table 3.3. Physical parameters of the used fluorophore and quencher [73]: The 0,0-energy E_{00}, lifetime of fluorophore, τ_F, quencher, τ_Q, reduction and oxidation potentials, $\boldsymbol{E_{1/2}^{red}}$ and $\boldsymbol{E_{1/2}^{ox}}$, respectively. The electron transfer driving force, $-\Delta G^0$, was calculated using the Rehm-Weller equation with Born correction assuming an inter-particle distance of 6.5 Å [37] and an ion radius of 3.25 Å at $\varepsilon_s = 13$ of propyl acetate/butyronitrile mixture.

F	E_{00} /eV	τ_F / ns[a]	$\boldsymbol{E_{1/2}^{red}}$ / V vs. SCE, ACN	$\boldsymbol{E_{1/2}^{ox}}$ / V vs. SCE, ACN	$-\Delta G^0$ ($\varepsilon_s = 13$) / eV[b]
DMAnt	3.07	13.0	-1.98	+0.95	0.28
Q	E_{00} / eV	τ_Q / ns	$\boldsymbol{E_{1/2}^{red}}$ / V vs. SCE, ACN	$\boldsymbol{E_{1/2}^{ox}}$ / V vs. SCE, ACN	
DMA	-	-	-	+0.81	

[a] taken from ref. 37 [b] taken from ref. 37

3.3.1. Micro-homogeneous binary solvents

Mixtures of propyl acetate (PA)/butyronitrile (BN) with varying static dielectric constant, ε_s, within a range from 6 to 24.7 were prepared according to: $\varepsilon(w_1) = w_1\varepsilon_1 + (1 - w_1)\varepsilon_2$ with w_i and ε_i denoting the weight fraction and dielectric constant of component *i* [1, 20, 41]. In these mixtures (Table 3.5), the viscosity (η = 0.58 cP), and thus, the diffusion coefficients are nearly constant (maximum variation of 1.2%). The refractive index (n = 1.383) is likewise almost invariant with solvent composition. The Pekar factor ($1/n^2 - 1/\varepsilon_s$) of PA/BN mixtures, which governs the outer-sphere electron transfer reorganization energy and, thus, the rate of ET processes, varies by only ±5% in the studied ε_s-range [31, 33].

3.3.2. Micro-heterogeneous binary solvents

The bulk dielectric constants, ε_s, of micro-heterogeneous toluene (TOL)/dimethylsulfoxide (DMSO) mixtures vary within a range from 4.3 to 15.5 via:

$\varepsilon_s = 62.5 \exp\left[-\frac{(1-x_{DMSO})}{0.78}\right] - 15.6$ with x_{DMSO} referring to DMSO mole fraction in micro-heterogeneous mixture. The solvent viscosity (η) and Pekar factor (γ) increase with increasing the DMSO concentration in TOL/DMSO mixtures (Table 3.6) [4, 6]. The solvent viscosity was determined from the Auslander model [74]. In Equation 3.2, with A_{21} = 0.7915, B_{12} = 0.0103 and B_{21} = 1.6998 were used [75].

$$\eta = \frac{\eta_1 x_1 (x_1 + B_{12} x_2) + \eta_2 [A_{21} x_2 (B_{21} x_1 + x_2)]}{x_1 (x_1 + B_{12} x_2) + [A_{21} x_2 (B_{21} x_1 + x_2)} \quad (3.2)$$

Here, the subscripts 1 and 2 refer to DMSO and TOL, respectively. η_i and x_i denote the viscosity and mole fraction of species *i*.

Table 3.4. Relevant solvent properties are given at 25 ^{0}C: density (ρ), static dielectric constant (ε_s), dynamic viscosity (η), refractive index (n). The solvent supplier and the purification methods are shown. Abbreviations: PA: propyl acetate, BN: butyronitrile, TOL: toluene, DMSO: dimethylsulfoxide. All parameters are taken from ref. 76.

Solvent	ρ / g mL^{-1}	ε_s	η / cP	n	Supplier	Purification
PA	0.888	6.0	0.58	1.383	Aldrich (99.5%)	distilled
BN	0.794	24.6	0.58	1.383	Fluka (99%)	distilled
TOL	0.862	2.4	0.55	1.494	Fluka (99%)	Distilled
DMSO	1.100	50.0	2.2	1.479	Aldrich (99.9%)	as received

Table 3.5. The dielectric constant mixture ($\varepsilon_{s,\ mix}$), mole fraction of butyronitrile (x_{BN}), viscosity (η), refractive index (n) and Pekar factor ($\gamma = (1/n^2 - 1/\varepsilon_s)$ of PA/BN mixtures.

$\varepsilon_{s,\ mix}$	x_{BN}	η / cP	n	γ
10	0.28	0.581	1.383	0.4228
12	0.41	0.581	1.383	0.4394
14	0.52	0.581	1.383	0.4513
16	0.63	0.581	1.383	0.4603
18	0.72	0.581	1.383	0.4672
20	0.81	0.581	1.383	0.4728
22	0.89	0.581	1.383	0.4773
24.7	1.00	0.581	1.383	0.4823

3.4. Sample preparation

The concentration of quencher was 0.06 M, while that of the fluorophore was 2.10^{-5} M. Samples were prepared in septa-sealed quartz cuvettes with 1 cm path length. In order to remove dissolved oxygen, all solutions were sparged with nitrogen gas for 15 minutes prior to addition of the quencher. The liquid quencher was added directly through the septum using a Hamilton syringe.

3.5. Apparatuses and measurements

3.5.1. Spectroscopy

Absorption spectra of the studied systems were recorded on Shimadzu UV-3101-PC UV-VIS-NIR spectrophotometer. The fluorescence spectra was measured on a thermostatted Jobin Yvo Fluoromax-2 spectrofluorimeter, sampling time: 1 s nm^{-1}. The temperature for fluorescence measurements was held T = 295 K with the control of a Haake F3 thermostat. Figure 3.4 shows the absorption and fluorescence spectra of the 9,10-dimethylanthracene (DMAnt) in the absence and presence of the quencher *N*,*N*-dimethylaniline (DMA) in propyl acetate

(PA)/butyronitrile (BN) and toluene (TOL)/dimethylsulfoxide (DMSO) mixtures at ε_s = 12 and ε_s = 7.3, respectively. The exciplex emission was extracted by using the model introduced in refs. 5, 77.

Table 3.6. The bulk dielectric constant (ε_s), mole fraction of DMSO (x_{DMSO}), viscosity (η), refractive index (n) and Pekar factor ($\gamma = (1/n^2 - 1/\varepsilon_s)$ of TOL/DMSO mixtures.

$\varepsilon_{s,\,mix}$	x_{BN}	η / cP	n	γ
4.3	0.10	0.5733	1.492	0.2163
5.3	0.14	0.5947	1.491	0.2606
6.3	0.18	0.6231	1.491	0.2909
7.3	0.21	0.6490	1.490	0.3129
8.3	0.25	0.6895	1.490	0.3297
9.8	0.29	0.7366	1.489	0.3486
11.5	0.34	0.8044	1.488	0.3641
13.0	0.39	0.8815	1.488	0.3746
14.5	0.43	0.9493	1.487	0.3829
15.5	0.45	0.9851	1.487	0.3875

3.5.2. Steady-state magnetic field effect measurements

Magnetic field effects on exciplex from steady-state measurements were recorded using thermostated cell (295 K) coupled to Jobin Yvon Fluoromax-2 spectrofluorimeter via light guides. The magnetic field in the sample compartment was measured using F. W. Bell Model 9200 Gaussmeter. A saturating magnetic field of 62 mT was applied. The earth magnetic field was not compensated, i.e., 'zero field' corresponds approximately 0.08 mT. The exciplex emission was detected at 550 nm for 60 s, time constant of 1 s. At each time, three measurements were accumulated, there by alternating zero and saturating magnetic field (Figure 3.5). The excitation slit width was 2 nm and the emission slit width 6 nm. All

fluorescence signals have been background corrected. Three repetitions were analysed independently and their maximum difference in magnetic field effect was given as experimental error [41]. The absolute MFE on the exciplex, χ_{SS}, are determined from time scans at the emission wavelength of the exciplex:

$$\chi_{SS} = \frac{\bar{I}(\lambda_{em}, B_{sat}) - \bar{I}(\lambda_{em}, B_0)}{\bar{I}(\lambda_{em}, B_0) - (\bar{I}_F(\lambda_{em}, B_0) - \overline{BG}(\lambda_{em}))I_c / I_0 - \overline{BG}(\lambda_{em})} \tag{3.3}$$

Here, $\bar{I}(\lambda_{em}, B_{sat})$ and $\bar{I}(\lambda_{em}, B_0)$ are the mean intensities at λ_{em} in a saturated magnetic field, B_{sat}, and in the absent magnetic field, B_0. $\bar{I}_F(\lambda_{em}, B_0)$ is the residual emission of the locally-excited fluorophore at λ_{em} in the absence of quencher. I_c and I_0 are the fluorescence intensities in the presence and absence of quencher. I_c/I_0 is the relative intensity of the prompt emission of the fluorophore in the presence of the quencher as obtained from the fluorescence spectra decomposition and $\overline{BG}(\lambda_{em})$ is the mean background intensity.

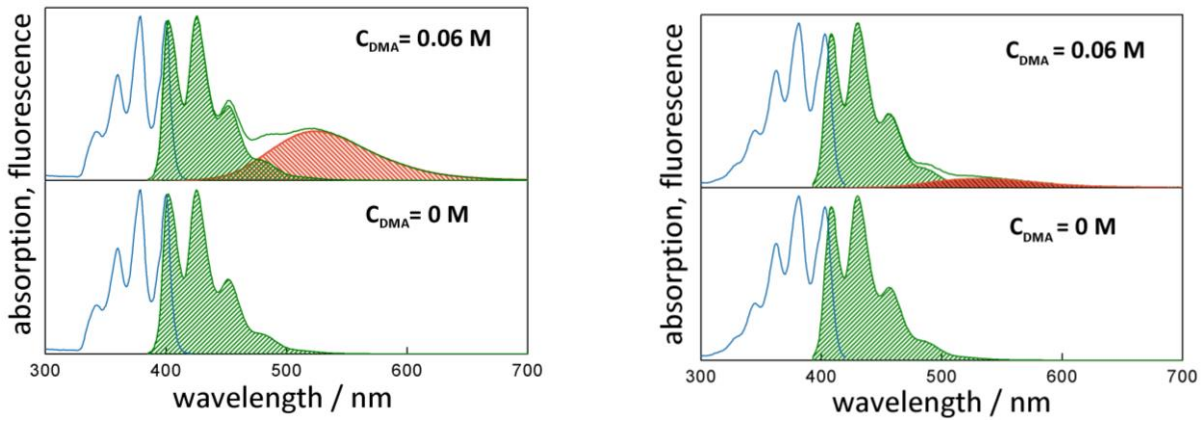

Figure 3.4. Absorption and fluorescence spectra of the 9,10-dimethylanthracene system in the mixtures of propyl acetate/butyronitrile mixture at ε_s = 12 (left panel) and toluene/dimethylsulfoxide mixture at ε_s = 7.3 in the absence and presence of quencher *N*,*N*-dimethylaniline (DMA).

3.5.3. Time-resolved magnetic field effect measurements

The setup used to record the time-resolved magnetic field effects (TR-MFE) on the exciplexes of the studied system is depicted in Figure 3.6. The TR-MFE of the 9,10-dimethylanthracene/*N*,*N*-dimethylaniline exciplex in TOL/DMSO mixture at ε_s = 6.3 is shown in Figure 3.7.

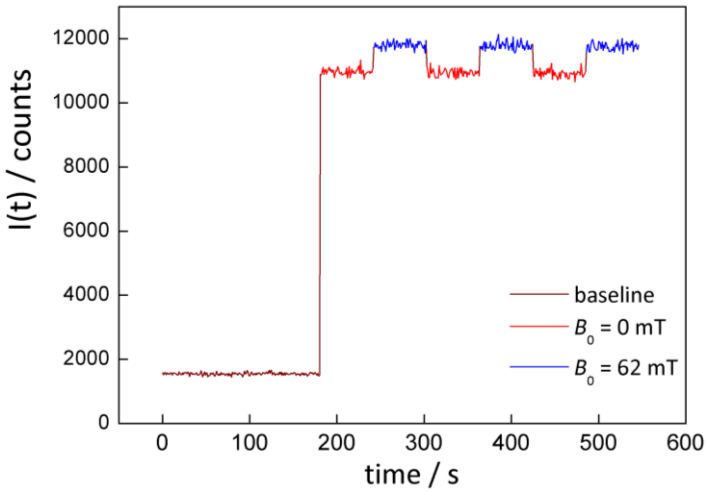

Figure 3.5. Time-dependent magnetic field effect on the 9,10-dimethylanthracene/*N*,*N*-dimethylaniline exciplex emission in steady-state measurements in the absence and presence of an external magnetic field. The exciplex emission was observed at 550 nm. Mixture of TOL/DMSO at ε_s = 11.5 was used a solvent.

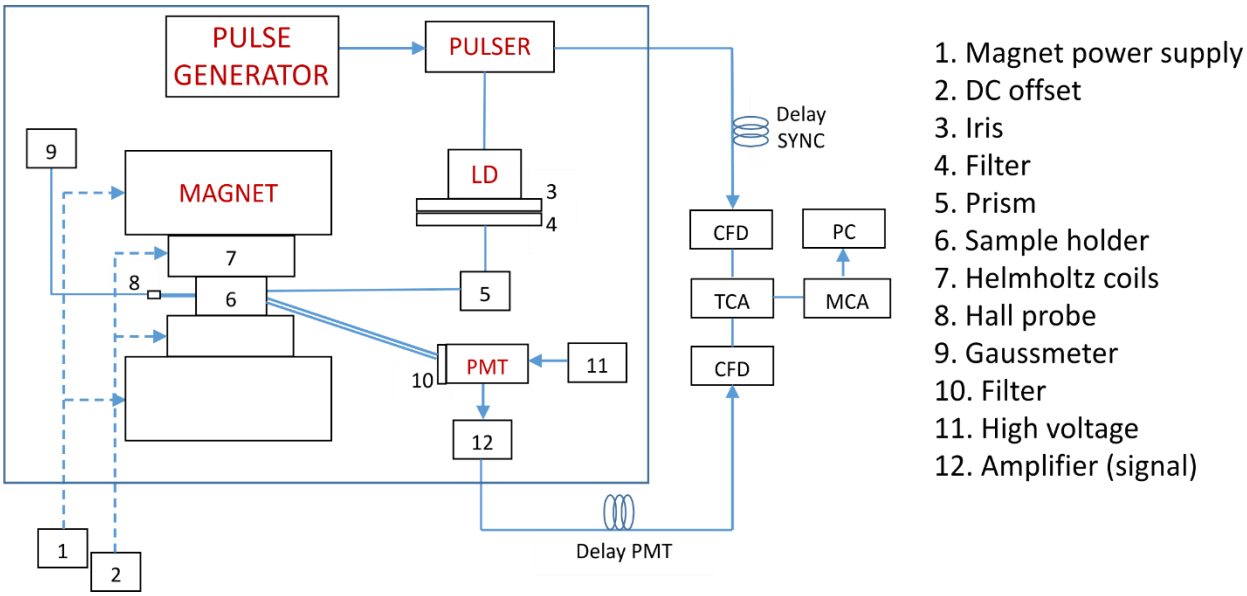

Figure 3.6. The setup used to record the time-resolved magnetic field effects of the exciplex of the studied system.

In order to record the exciplex decay as a function of time, the light source was driven by pulse (Stanford Research Systems, INC, Model DG-535) with a repetition rate of 0.8 MHz. The pulser also serves to generate the so-called SYNC signal being the start signal for the time-to-amplitude converter (TAC). As the signal is generated electronically, no constant

fraction discriminator (CFD) has been used in the SYNC channel. The light source used for excitation of the sample was a 374 nm laser diode (Picoquant, LDH series, Pulse FWHM 60 ps). Right in front of the light source, an excitation filter [**4**] (UG1) was placed. The intensity of the light source was adjusted via an iris [**3**]. A prism [**5**] is placed to refract the excitation light to the cuvette [**6**], where the sample is excited. The sample itself is contained in a thermostattable sample holder which is located between the pole shoes of an electromagnet. The radiation emitted by the sample is transported to the detector. A high voltage [**11**] driven photomultiplier tube (PMT, Hamamatsu, R5600-U04) in combination with a non-fluorescing emission filter LP550 [**10**] is used to detect the optical signal. Its output delivers the stop pulse for the TAC (Ortec, model 567). As the amplitude of the PMT output signal is only in the range of some 20 mV, a pre-amplifier [**12**] (Ortec, VT120) is used before the signal is transferred to the constant fraction discriminator (CFD). At the TAC the information from the two signal paths is evaluated and transferred to the multi-channel analyser (Ortec, EASY-MAC) where the histogram of single photon events is generated. To study the influence of magnetic field on the reaction, a magnet power supply [**1**] in combination with the Helmholtz coils [**7**] and a DC offset [**2**] have been used to adjust the magnetic field strength. On the gaussmeter [**9**] the actual field value sensed by the hall probe [**8**] is read off. All TR-MFE measurements have been performed at 295 K and the time-resolved exciplex emission data were recorded using the Time-Correlated Single Photon-Counting (TCSPC) technique. The sample was immersed in the magnetic field of a Bruker B-E10B8 electromagnet. The saturating external magnetic field was set to B_0 = 0 mT to 62 mT.

The decay kinetics of exciplex includes the dissociation into free ions and recombination giving rise to delayed exciplex emission. The difference in the exciplex emission intensity, ΔI(t), in the presence and absence of an external magnetic field in time-resolved MFE (TR-MFE) measurement is given by:

$$\Delta I(t) = I(t, B_0) - I(t, B_0 = 0) \tag{3.4}$$

Here $I(t, B_0)$ and $I(t, B_0 = 0)$ are time-resolved intensities of the exciplex decays in the presence and absence of an external magnetic field. After matching their amplitudes within the first nanosecond which has no significant MFE. Integrating the time traces according eq. (3.3) with $t_{max} \rightarrow \infty$ to determine the MFE on the exciplex, χ_{TR}, in time-resolved MFE measurements:

$$\chi_{TR} = \frac{\int_0^{t_{max}} \Delta I(t)dt}{\int_0^{t_{max}} I(t, B_0 = 0)dt} \tag{3.5}$$

Here, t_{max} in the range from 200 to 500 ns was integrated depending on the solvent polarity.

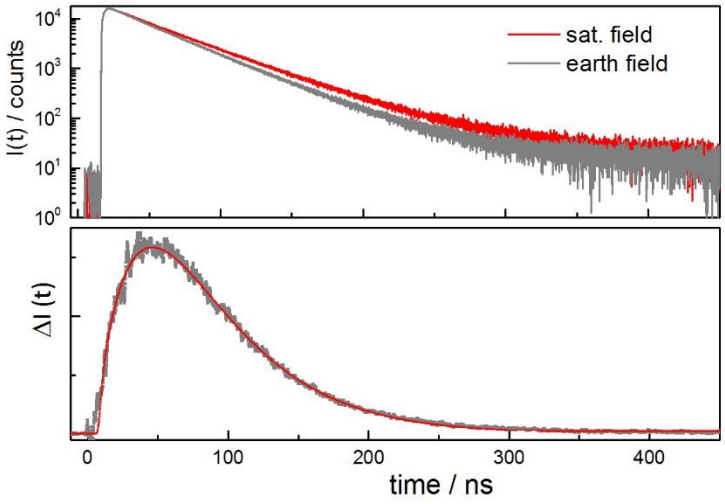

Figure 3.7. Exciplex emission decays (upper panel) of the 9,10-dimethylanthracene (2.10^{-5} M)/*N*,*N*-dimethylaniline (0.06 M) system in TO/DMSO mixture at ε_s = 6.3 in the absence (grey curve) and presence (red curve) of a saturating external magnetic field (62 mT) observed with a long-pass filter LP550 nm after excitation at 374 nm by a laser pulse. The delayed exciplex emission is enhanced in a saturating external magnetic field effect. The lower panel refers to time-evolution magnetic field effect ΔI(t) (grey scattered curve) obtained from eq. (3.4) and its simulation (red solid curve).

4. RESULTS AND DISCUSSION

4.1. The solvent property dependence of magnetic field effect of the exciplex

In this investigation, the fluorophore (F)/quencher (Q) pair selected consists of 9,10-dimethylanthracene (DMAnt) that acts as an electron acceptor and of *N*,*N*-dimethylaniline (DMA) as an electron donor. Mixtures of propyl acetate (PA)/butyronitrile (BN) with varying the static dielectric constants, ε_s, within a range from 6 to 24.7 were selected as micro-homogeneous binary solvents. Toluene (TOL)/dimethylsulfoxide (DMSO) mixtures were used as micro-heterogeneous solutions with ε_s in the range from 4.3 to 15.5 (see the experimental part for details on sample and solvent preparations).

Upper panel in Figure 4.1 depicts the solvent polarity dependence of time-resolved magnetic field effects (TR-MFEs), χ_{TR}, determined by integration according to eq. (3.5) from the time-resolved data in TOL/DMSO mixtures in comparison to steady-state MFEs, χ_{SS}, obtained from steady-state measurements. The agreement of χ_{TR} and χ_{SS} values indicated that under low light intensity and low concentration of the fluorophore conditions in TR-MFE measurements, no bulk processes, i.e., reencountering ions in the bulk, and processes involving fluorophore triplets contribute to the MFEs observed. MFEs on the exciplex can only be due to the effect of an external magnetic field on S-T mixing in geminate RIPs [21].

MFE features have been analysed in terms of $\varepsilon_{s,\,onset}$, $\varepsilon_{s,\,max}$ (ε_s values showing the onset and maximum of MFE, respectively), x_{onset}, x_{max} (mole fraction values of polar component in binary solvent showing the onset and maximum of MFE) and χ_{max} (the maximum MFE obtained). Table 4.1 gives the above parameters in two binary solvents. The onset and maximum of MFEs obtain at smaller ε_s values in TOL/DMSO mixture. The maximum MFE value (χ_{max} = 14.5%) appears at ε_s = 8.3 in micro-heterogeneous solutions while that obtains at ε_s = 18 (χ_{max} = 12.2%) in micro-homogeneous ones. As mentioned above, RIP dynamics may reflect altered MFEs. The environment around RIP changes with the change in the composition of the solvent mixtures. According to Suppan's model, the polar micro-domains (DMSO or BN) around solute species (RIP or exciplex), the dielectric enriched region, are

produced via ion-dipole and dipole-dipole interactions of solute molecules with the polar components [62, 78]. In micro-heterogeneous environment, DMSO molecules get preferentially favoured in the solvation shell, forming micro-clusters surrounding the RIP [28, 67, 68, 78-80]. The results have been published in ref. 6, the authors used the dielectric continuum model suggested by Basilevsky et al [65] to simulate the local concentration of DMSO, y(r), surrounding RIP in TOL/DMSO mixtures (r is inter-radical separation) (see Figure 4.2). The polar micro-domains are surrounding ions and the space in between ions. Irrespective of DMSO concentration in mixtures, the ions are covered by a layer of DMSO (y = 1). This solvation effects on RIP lifetimes and induces an effective compromise between separation and recombination in geminate radical ion pairs [6]. Thus, MFEs appear and reach the maximum value at smaller ε_s in TOL/DMSO solutions.

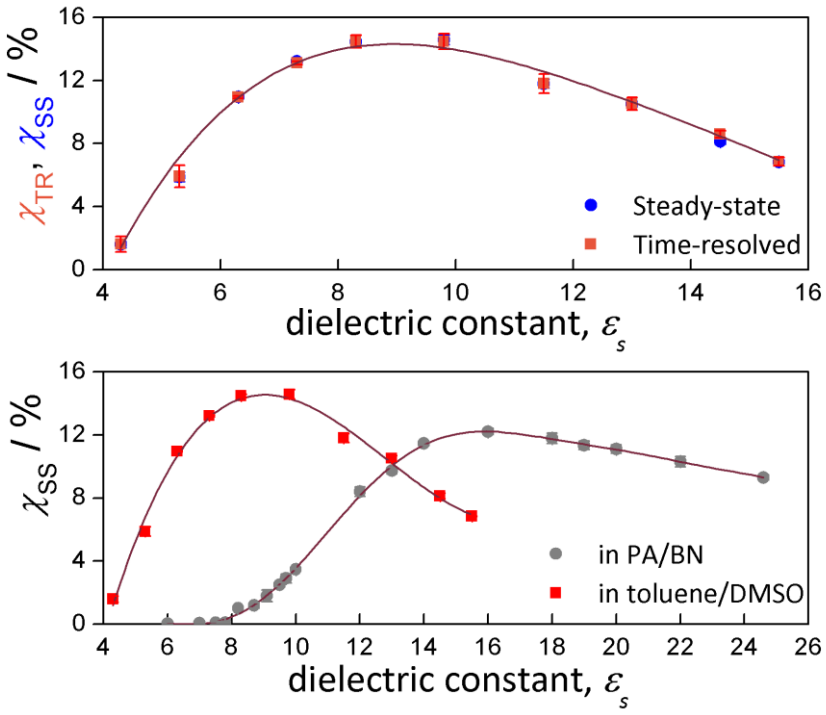

Figure 4.1. Upper panel: The magnetic field effects on DMAnt/DMA exciplex determined from TR-MFE (orange squares with error bars) and steady-state (blue circles) in TOL/DMSO with various ε_s. Lower panel gives steady-state MFEs of the exciplex in TOL/DMSO (red squares) mixtures in comparison to those in PA/BN (grey circles) ones in the studied ranges of ε_s.

After reaching the maximum value, MFEs decrease with increasing the solvent polarity. The effect of solvent polar components reaches saturation with increasing their mole fraction in mixture. At high ε_s values, i.e., high mole fractions of BN and DMSO in the corresponding mixtures, the separation of the two radicals in RIP is favourable, but the radical reencounter probability in the geminate cage is not sufficient due to the prevention from solvent polar components (BN or DMSO) in solution. This results in a decrease in MFEs.

Table 4.1. The parameters used to analyse the MFEs of 9,10-dimethylanthracene/*N*,*N*-dimethylaniline exciplex in micro-homogeneous and micro-heterogeneous binary solvents. Abbreviation: PA: propyl acetate, BN: butyronitrile, TOL: toluene, DMSO: dimethylsulfoxide.

Solvent	$\varepsilon_{s,\,onset}$	x_{onset}	$\varepsilon_{s,\,max}$	x_{max}	χ_{max} (%)
PA/BN	8.0	0.15	18.0	0.72	12.2
TOL/DMSO	4.3	0.10	8.3	0.25	14.5

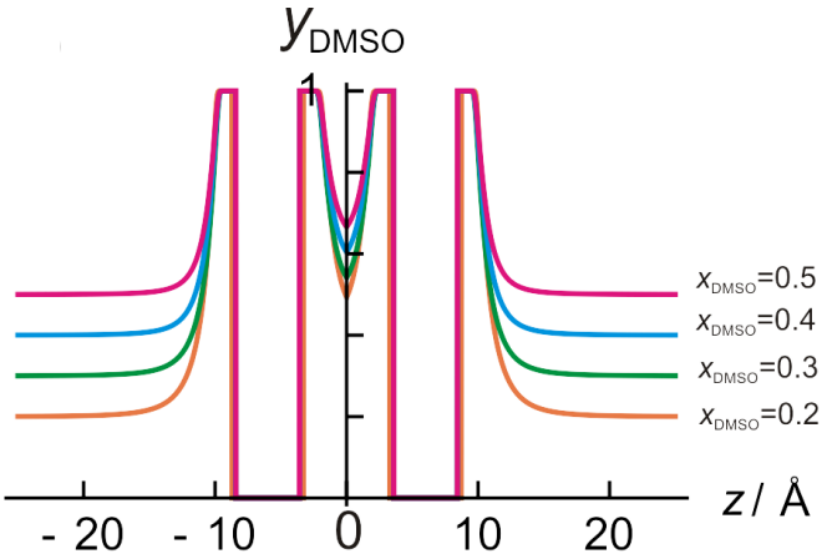

Figure 4.2. Simulations of the local concentration of DMSO at various mole fraction of DMSO. The graph gives slices through the centers of two ions and *y*(r) shows axial symmetry. The inter-radical separation is 10 Å. The space axis is given by *z*.

4.2. The initial quenching product and exciplex kinetics dependence on the preferential solvation of polar components in binary solvents

Time-resolved data of the MFEs on the exciplexes of 9,10-dimethylanthracene/*N*,*N*-dimethylaniline system were carried out by TCSPC technique in micro-homogeneous and micro-heterogeneous binary solvents . In order to investigate the effect of an external magnetic field on the delayed exciplex fluorescence (Figure 3.7), time-resolved MFEs (TR-MFEs) of the exciplex are measured in the absence (B_0 = 0 mT) and presence of a saturating external magnetic field (B_0 = 62 mT). The time traces rise with a time constant of 1.8 ns, and are almost independent on the magnetic field. The decay kinetics of exciplex includes the dissociation into free ions and recombination giving rise to delayed exciplex emission. The difference in the exciplex emission intensity, ΔI(t), in the presence and absence of an external magnetic field in TR-MFE measurement is given by eq (3.4).

The time-resolved MFEs for various dielectric constants in PA/BN and TOL/DMSO mixtures are shown in Figure 4.3 and 4.4 with simulations. No MFE is detected with the first two nanoseconds of the experiments. The maximum of the TR-MFEs occurs in the range from 10 to 75 ns after excitation, with larger values occurring at lower dielectric constants. The delayed exciplex fluorescence decays reach the noise level of the experiment within 400 ns.

As noted above, RIP formation via distant ET or via exciplex dissociation depends on the properties of solvent environment. Since the exciplex dissociation is usually a slow process, the ions resulting from exciplex dissociation will be delayed with respect to RIPs formed by distant electron transfer. As a consequence the MFE generated by the exciplex route will also be delayed, i.e., time-resolved MFEs occurs at longer time-scale. In micro-homogeneous PA/BN (Figure 4.3) and micro-heterogeneous TOL/DMSO (Figure 4.4) solutions, time-resolved-MFEs of the exciplex occur in shorter time-scale with increasing the static dielectric constants, ε_s. These results indicated that in higher bulk dielectric constant solutions, the RIPs generated via distant electron transfer (pathway B2 in Scheme 2.1) are dominant, to be discussed below.

In micro-heterogeneous environment, the polar component (DMSO) in solvent mixtures is crucial in deciding the initial quenching products, i.e., exciplexes or RIPs. The maximum of ΔI(t) in TOL/DMSO mixture occurs at shorter time-scale in comparison to the iso-dielectric constant in PA/BN mixture (Figure 4.5). The RIP formation in ET deactivation is exclusive in the presence of DMSO molecules in solution. The preferential solvation of DMSO molecules around RIPs is more efficient than BN molecules. This leads to the RIP formation with higher

ratio, in agreement with time-scales of TR-MFEs. Furthermore, the viscosity of micro-heterogeneous solution increases with increasing the DMSO mole fraction (Table 3.6) and the fluorescence quenching occurs predominantly by distant ET channel with increasing the solution viscosity.

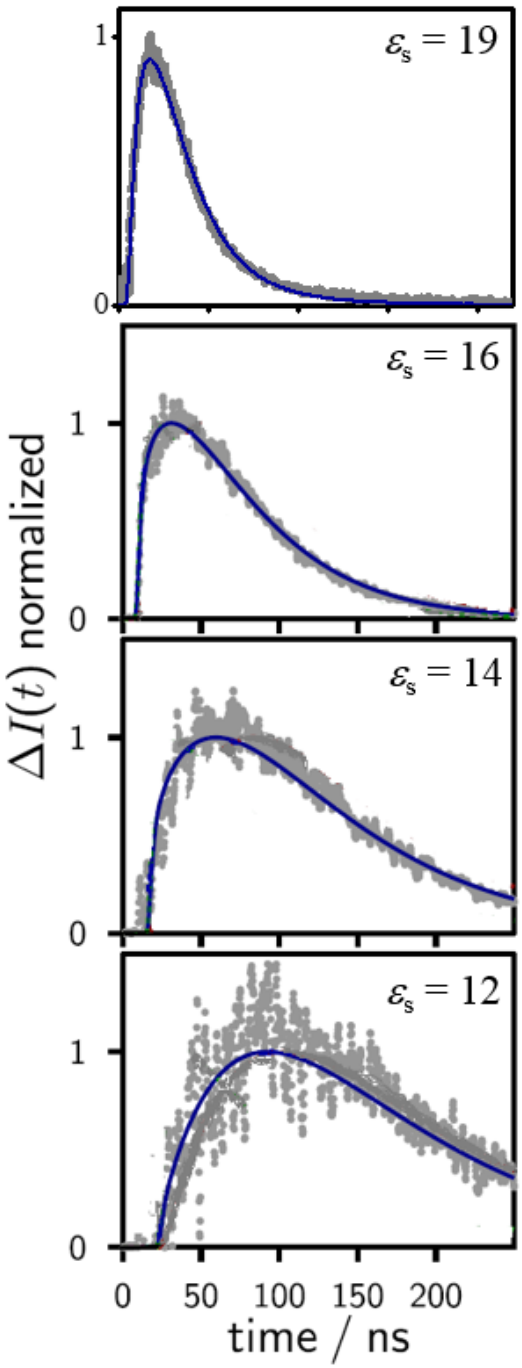

Figure 4.3. Experimental time-dependent magnetic field effects at different dielectric constants, ε_s, in PA/BN mixtures for the DMAnt/DMA exciplex. The grey scatter and the blue solid curves refer to the experimental and simulation curves, respectively.

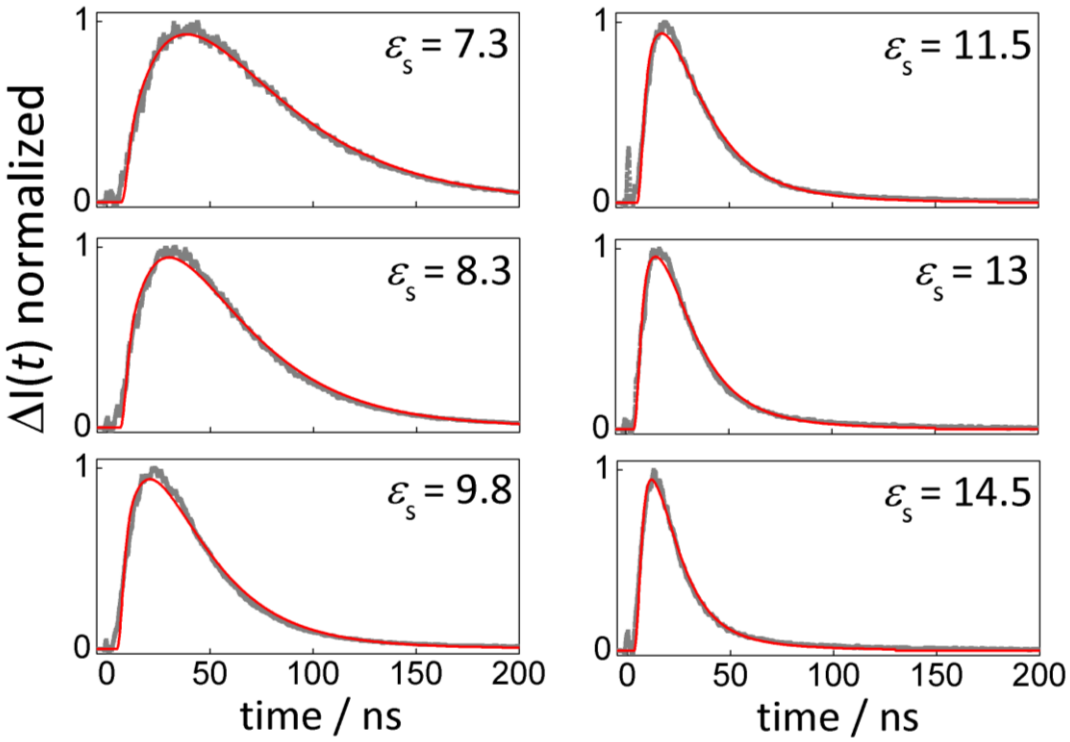

Figure 4.4. Experimental time-dependent magnetic field effects at different dielectric constants, ε_s, in TOL/DMSO mixtures for the DMAnt/DMA exciplex. The grey scatter shows the experimental data and their simulations are shown in red solid curves.

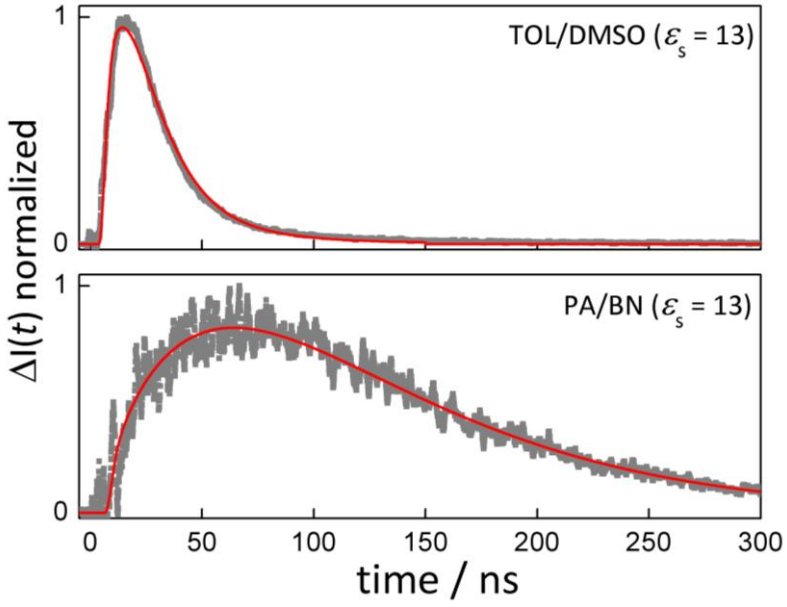

Figure 4.5. The time-resolved magnetic field effects of the exciplexes for the DMAnt/DMA system in TOL/DMSO mixture at ε_s = 13 (upper panel) in comparison to the iso-dielectric constant PA/BN mixture (bottom panel).

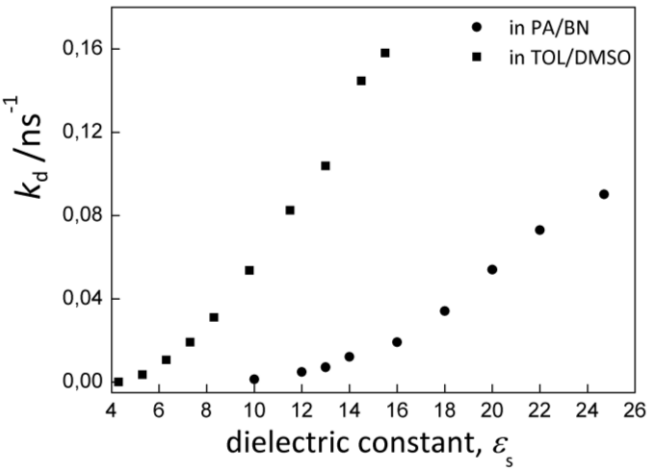

Figure 4.6. The dependence of exciplex dissociation rate constant, k_d, of the DMAnt/DMA system on static dielectric constant, ε_s of PA/BN (circles) and TOL/DMSO (squares) mixtures.

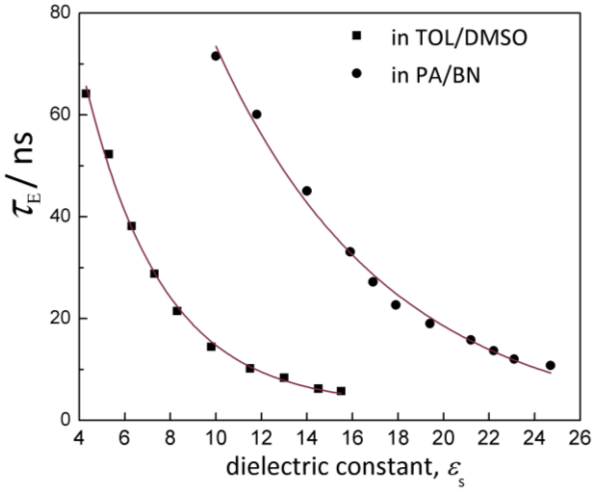

Figure 4.7. Solvent polarity dependence of the exciplex lifetimes of the DMAnt/DMA system in PA/BN (circles) and TOL/DMSO (squares) mixtures.

The exciplex kinetics is evaluated through the association constant $K_a = k_a / k_d$ (where k_a and k_d are the rate constants of RIP association into exciplex and exciplex dissociation into RIP, respectively) (Figure 4.6) and the exciplex dissociation quantum yield $\phi_d = k_d \tau_E$ (see appendix A2). ϕ_d was estimated from the dependence of exciplex lifetime, τ_E, on dielectric constants [1, 20]. The τ_E values were extracted from the initial decay of the exciplex emission at each ε_s scanned. The solvent dependence of τ_E is described in Figure 4.7. K_a and ϕ_I (the probability that the initial state is the loose ion pair (pathway B2 in Scheme 1). Thus, (1 - ϕ_E) is the

probability that the exciplex formed initially (pathway B1 in Scheme 1)), have a strong effect on the shape and the magnitude of the time-resolved MFEs [1, 20]. Using a model including the exciplex dissociation, the spin evolution of the geminate pair and its reencounter (eq. 3.1) [1, 20], the parameters K_a and ϕ_I can be determined by fitting the experimental MFE data. Figure 4.8 shows the dependence of K_a, ϕ_d and ϕ_I as functions of dielectric constants in two binary solvents studied.

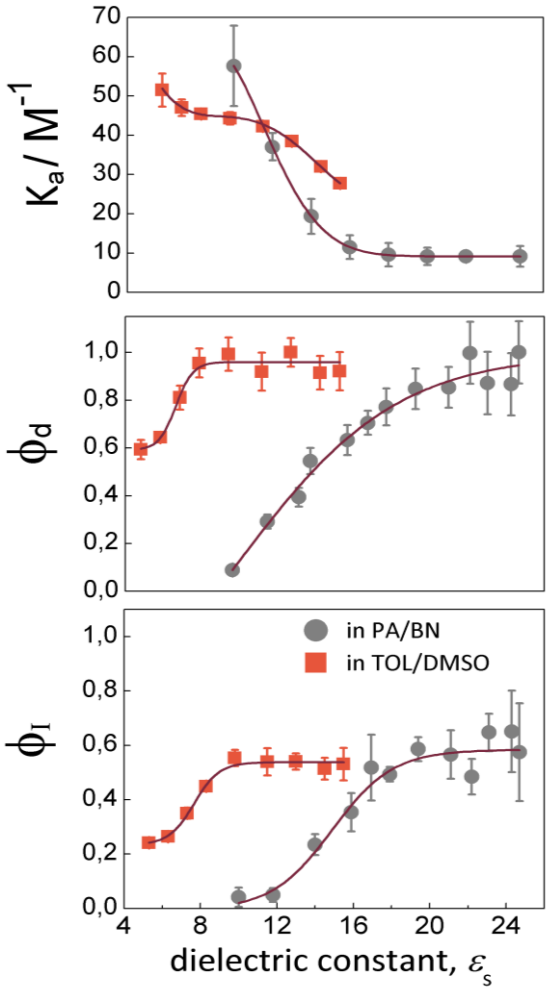

Figure 4.8. The solvent polarity dependence of the association constant (K_a, top panel), the exciplex dissociation quantum yield (ϕ_d, center) and the initial probability of the radical ion pair (ϕ_I, bottom) of the DMAnt/DMA system in PA/BN (grey circles with error bars) and TOL/DMSO (orange squares with error bars) mixtures. The solid curves are to guide the eye.

The plot of above parameters (K_a, ϕ_d, ϕ_I) as functions of solvent polarity shows, firstly, that the enrichment of polar components (DMSO or BN) in solvation shell surrounding solute species mainly governs the separation of the exciplex into the ions. That is reflected in the

trend of K_a and ϕ_d with increasing the mole fraction of polar component in solvent mixtures. Secondly, that the reaction mechanism dependence on the bulk dielectric constant and the preferential solvation effect is clarified. The mechanism is reflected through ϕ_I values which refer to the initial probability of the radical ion pair (pathway 2B in Scheme 2.1). In TOL/DMSO solutions, within experimental error, the exciplex dissociation quantum yield reaches unity ($\phi_d = 1$) at $\varepsilon_s = 8.3$ onwards while that will be obtained from $\varepsilon_s = 22$ in PA/BN mixtures. These results can be explained by the effect of the environment around the exciplex. The local DMSO concentration increases with increasing its mole fraction in mixture. The micro-cluster formation of polar molecules surrounding the charge-transfer dipoles (exciplexes) governs exciplex kinetics (exciplexes dissociate into RIPs).

The data summarized in the bottom panel in Figure 4.8 shows that the probability of distant ET quenching (ϕ_I) increases with increasing polarity of the solution. This result is also reflected through a decrease in lifetime of locally-excited fluorophore (Figure 4.9). After light absorption, electron transfer with a quencher (Q) is one of ways to deactivate of an excited fluorophore (F*). F* and Q approach each other by diffusion. During the lifetime of F*, if a distant ET occurs, the excited fluorophore will deactivate to ground state faster, i.e., its lifetime decreases. ϕ_I levels off at ε_s exceeding 9.8 and 20 in TOL/DMSO and PA/BN mixtures, respectively. For the investigated dielectric constant range, ϕ_I is less than unity, i.e., the direct exciplex formation (pathway B1 in Scheme 2.1) contributes at all dielectric constants in micro-homogeneous and micro-heterogeneous environments. Detection of exciplex luminescence was limited to the ε_s range where exciplex emission is sufficient. As expected, the exciplexes are dominantly formed at low polarities. This observation is in agreement with the model introduced in ref. 5, the exciplex is more stabilized due to the less shielded Coulomb interaction of $Q^{+\cdot}$ and $F^{-\cdot}$ in less polar solutions. In polar environment, such as acetonitrile, the exciplex can simultaneously contribute on the quenching reaction [56, 57, 80-82]. Here, exciplex contribution was still observed even at $\varepsilon_s = 15.5$ in micro-heterogeneous TOL/DMSO mixture and at $\varepsilon_s = 24.7$ in pure butyronitrile. In micro-heterogeneous mixtures, the viscosity of the environment increases with increasing the DMSO concentration [75] while that is independent from composition in PA/BN mixtures [1, 6, 20]. The loose-ion channel will be significant with increasing solvent viscosity. On the other hand, if an locally-excited fluorophore (F*) and quencher (Q) approaching each other by diffusion to form a favourable stacked configuration facilitating exciplex is faster than the

distant ET, the exciplex channel can contribute on the quenching process. This approach occurs in both solvent mixtures. The direct formation of RIPs is more favoured in polar solutions. The quenching reaction occurs through the LIP formation. With an increase the mole fraction (DMSO) from 0.2 to 0.5, the potentials of mean force (PMF) profiles (see Figure 4.10), a function of the inter-particle separation, show that in the region of the inter-radical separation of 10 Å of RIP, the barrier to radical separation is in the order of k_BT. This induces a stabilized RIP in polar solutions [6]. The enrichment of DMSO molecules in the solvation shell surrounding RIPs drives ϕ_I to level off at smaller ε_S values in micro-heterogeneous solutions.

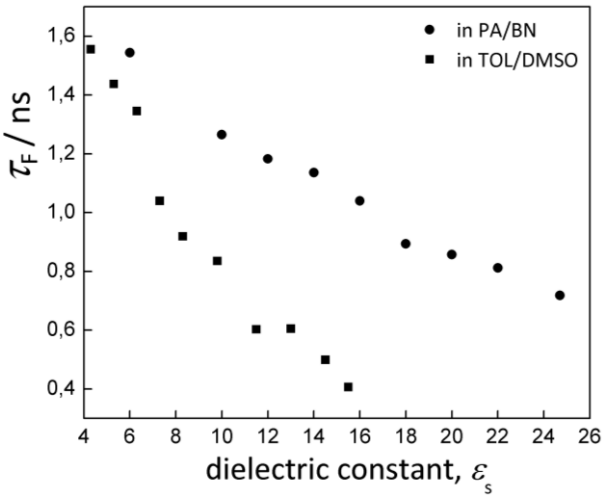

Figure 4.9. Solvent dependence of the lifetime of the locally excited fluorophore in PA/BN (circles) and TOL/DMSO (squares) mixtures.

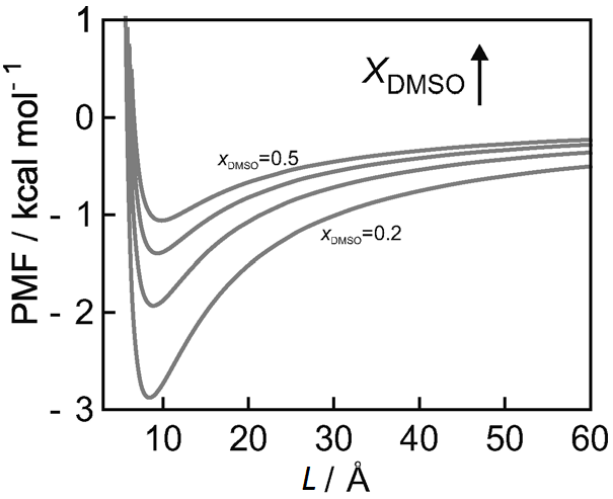

Figure 4.10. Potentials of mean force (PMF) at various DMSO mole fractions (x = 0.5, 0.4, 0.3, 0.2). PMF is calculated from the continuum solvation model (see experimental section).

4.3. The exciplex emission band and the sovatochromic effect on the exciplex emission in binary solvents

Figure 4.11 depicts the red-shift of the exciplex fluorescence of the 9,10-dimethylanthracene/*N*,*N*-dimethylaniline system in PA/BN and TOL/DMSO mixtures. The exciplex emission proceeds vertically giving rise to the dissociative ground state (Scheme 2.1).

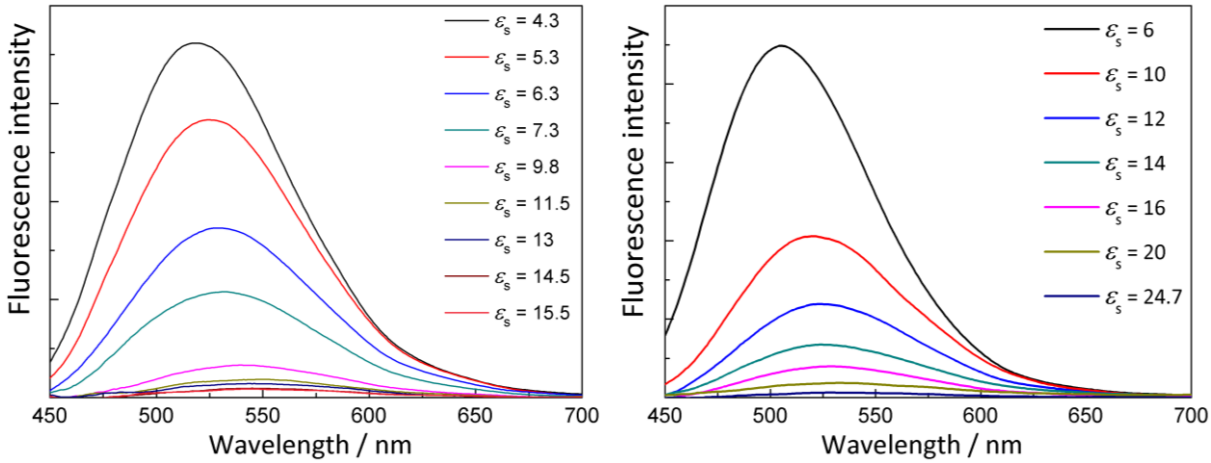

(a) In PA/BN mixtures (b) In TOL/DMSO mixtures

Figure 4.11. The exciplex emission bands of the exciplex of the DMAnt/DMA system at different bulk dielectric constants, ε_s, in PA/BN (a) and TOL/DMSO (b) mixtures. The maximum wavelengths of exciplex emission bands are shifted with increasing the ε_s values.

The exciplex emission bands shift to lower energies with increasing solvent polarity, in agreement with the model of self-consistent polarization of the medium [70, 83]. On the other hand, the Stokes shift in binary solvents can be explained by the preferential solvation of the polar components [67, 84]. After excitation, the locally-excited fluorophore and quencher approach each other by diffusion, under a well-defined relative orientation [8-11], the excited-state charge-transfer complex (exciplex) will be formed. This complex has a dipole moment. The polar solvent molecules generate a cluster (solvent shell) surrounding the dipole solute molecules due to diffusion of the polar molecules from the bulk of the solvent mixture. This causes a difference between the effective dielectric constant, ε_{eff}, around the exciplex and the bulk dielectric constant, ε_s. Concentration of the polar solvent molecules in the cluster depends on their mole fraction in mixture. The dielectric enrichment around the exciplex

increases with increasing the concentration BN or DMSO. This effect is reflected in the exciplex emissions which shifted to longer wavelength. In particular, in micro-heterogeneous mixture of TOL/DMSO, the presence of the DMSO (high polar component) molecules in the solvent shell gives rise to the significant red-shift in comparison to the iso-bulk dielectric constant of micro-homogeneous mixture of PA/BN (Figure 4.12).

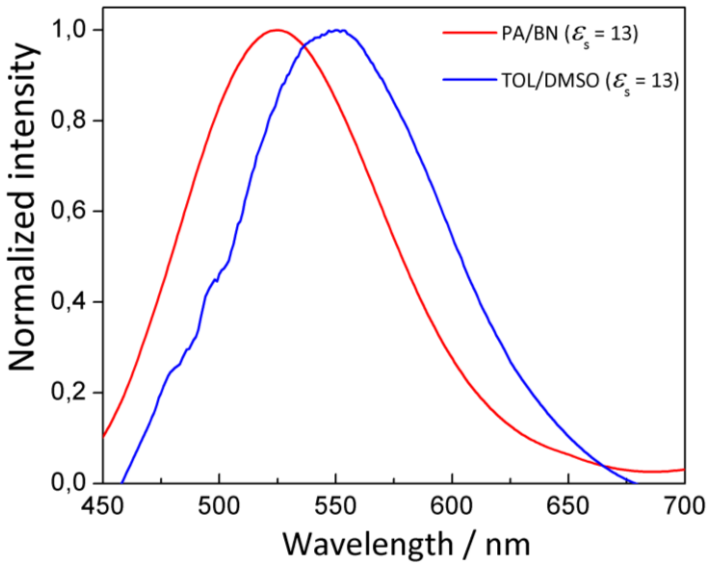

Figure 4.12. The exciplex emission band of the DMAnt/DMA exciplex in PA/BN (red) and TOL/DMSO (blue) mixtures at ε_s = 13.

5. CONCLUSIONS AND OUTLOOKS

5.1. Conclusions

In this work, we have utilized the time-resolved MFE measurements of the exciplex of 9,10-dimethylanthracene/*N*,*N*-dimethylaniline system in micro-homogeneous and micro-heterogeneous mixtures with varying the static dielectric constants, ε_s. The onset and maximum magnetic field effects of the exciplex occur at smaller ε_s values in micro-heterogeneous environment TOL/DMSO. The maximum of the TR-MFEs of the exciplexes occur at shorter time-scales with increasing the solvent polarity in both binary solvents. In particular, the maximum of ΔI(t) in TOL/DMSO mixture occurs at shorter time-scale in comparison to the iso-dielectric constant in PA/BN mixture. All these results can be attributed to the preferential solvation of polar components (BN and DMSO) in mixtures. They form a polar cluster around solute molecules (exciplex, RIP) due to dipole-dipole interaction. With the presence of the high polar component DMSO in the polar cluster, the effects on the resulting observations are more significant.

By using the reversible model which accounts for the initial quenching products and the exciplex dissociation were taken into account to simulate experimental data, the exciplex kinetics and the mechanism of fluorescence quenching are clarified. The exciplex kinetics and the initial quenching products depend strongly on the solvent property. In both micro-homogeneous and micro-heterogeneous environments, the probability of the initial formation of RIP is always less than unity, i.e., the exciplex formation contributes in all ε_s studied. The exciplex formation is dominant in less polar solutions. The direct RIP formation is more favourable in higher polarity. In particular, in micro-heterogeneous solutions, the local concentration of DMSO in solvation shell around exciplexes and RIPs plays an important role in the exciplex kinetics and in deciding the initial quenching products. Finally, as far as the applicability of the work is concerned, the results successfully demonstrated that the time-resolved MFE studies have the potential to provide the detailed insights of the reaction dynamics of RIPs and exciplexes.

5.2. Outlooks

- In this thesis, there have been left space for more experiments. The initial quenching products should be observed by transient absorption spectroscopy in time-scales of picosecond or femtosecond.
- The effect of solvent viscosity on the RIP and exciplex formation would continue. Finding out a larger range of solvent viscosity in which the MFE on the exciplex can observe significantly is a challenge.

A. APPENDIX

A1. Unit conversion

Energy in eV:	1 eV = 96.485 $kJmol^{-1}$ = 8065.5 cm^{-1}
Time in ns:	1 ns = 10^{-9} s
Length in Å:	1 Å = 10^{-10} m
Unimolecular rate constant in ns^{-1}:	1 ns^{-1} = 10^{9} s^{-1}

A2. Formulation of the exciplex dissociation quantum yield, ϕ_d

Micro-homogenous binary solvents PA/BN:

The exciplex lifetime is a function of the static dielectric constant, ε_s, and is defined by:

$$\tau_E(\varepsilon_s) = \frac{1}{k_r + k_{nr} + k_d(\varepsilon_s)} \tag{A2.1}$$

where k_r, k_{nr} are the rate constants of the radiative and non-radiative exciplex decays, respectively. k_d gives the exciplex dissociation rate constant (pathway C in Scheme 2.1).

At $\varepsilon_s = 6$, under the assumption that there is no exciplex dissociation, i.e., $k_d = 0$.

Inserting $k_d = 0$ in eq. (A3.1) yields

$$k_r + k_{nr} = \frac{1}{\tau_E(\varepsilon_s = 6)} = const \tag{A2.2}$$

From eq. (A2.1) and eq. (A2.2), k_d is calculated by:

$$k_d(\varepsilon_s) = \frac{1}{\tau_E(\varepsilon_s)} - \frac{1}{\tau_E(\varepsilon_s = 6)} \tag{A2.3}$$

The exciplex dissociation quantum yield is defined by:

$$\phi_d(\varepsilon_s) = \frac{k_d(\varepsilon_s)}{k_d(\varepsilon_s) + k_r + k_{nr}} \tag{A2.4}$$

Introducing eq. (A2.3) in eq. (A4.4) yields

$$\phi_d(\varepsilon_s) = k_d(\varepsilon_s).\tau_E(\varepsilon_s) \tag{A2.5}$$

Micro-heterogeneous binary solvents TOL/DMSO:

Under an assumption that there is no exciplex dissociation at $\varepsilon_s = 4.3$, i.e., k_d ($\varepsilon_s = 4.3$) = 0. The same argument applied for PA/BN mixtures will result in the eq. (A2.5).

A3. Calculations of the Singlet Probability / and the Recombination Function:

The singlet probability $\rho_S(t, B_0)$ is given by:

$$\rho_S(t, B_0) = Tr\left[\hat{P}_S \hat{\rho}(t, B_0)\right] \tag{A3.1}$$

Where $\hat{P}_S$ refers to the singlet projection operator, *Tr* is the trace operator, and the time behavior of the spin density matrix $\hat{\rho}(t, B_0)$ is obtained from the Liouville-von-Neumann equation:

$$\frac{d\hat{\rho}}{dt} = -i\left[\hat{H}, \hat{\rho}\right] + \hat{\hat{K}}_{ex}\hat{\rho} \tag{A3.2}$$

With the initial density matrix given by:

$$\hat{\rho}(t=0) = \frac{\hat{P}_S}{Tr(\hat{\rho})} \tag{A3.3}$$

In the low-viscosity approximation, the exchange interaction can be neglected, thus, the Hamiltonian $\hat{H}$ for a single radical *i* only contains contributions from the Zeeman interaction of the electron spins and the hyperfine interactions according to:

$$\hat{H}_i = g_i \mu_B B \hat{S}_{i,z} + \sum_j a_{ij} \hat{S}_i \hat{I}_{ij} \tag{A3.4}$$

Since only moderate magnetic fields are employed, it is furthermore assumed that $g_1 = g_2 = 2.0023$. The influence of the exchange operator $\hat{\hat{K}}_{ex}$ accounting for degenerate electron exchange is then calculated from:

$$\hat{\hat{K}}_{ex}\hat{\rho} = \frac{1}{\tau_{ex}}\left[Tr_n(\hat{\rho}) \otimes \frac{\hat{1}}{N} - \hat{\rho}\right] \tag{A3.5}$$

In this work, the spin correlation tensor approach was used to calculate the singlet probability (Figure 3.2). This approach implies a reformulation of Equations (A3.2, A3.3, A3.5) which allows a more efficient numerical treatment of the problem in Hilbert space. For the pseudo first-order self-exchange rate constant, $k_{ex} = 1/\tau_{ex}$, a value of τ_{ex} = 8 ns was used in all simulations.

The singlet yields are calculated from:

$$R(t, B_0 \mid r_I) = \int_0^t \rho_S(t, B_0)\, f(t \mid r_I) \exp\left(-\frac{t}{\tau_R}\right) dt \tag{A3.6}$$

With $f(t \mid r_I)$ denoting the recombination flux, and τ_R the radical pair lifetime. The recombination flux is the defined as:

$$f(t \mid r_I) = k_a n(r_E, t \mid r_I) \tag{A3.7}$$

With the time-dependence of $n(r,t)$ given by:

$$\frac{\partial n(r,t)}{\partial t} = \frac{1}{r^2}\frac{\partial}{\partial r} D(r) r^2 \exp(\frac{r}{r_c}) \frac{\partial}{\partial r} \exp(-\frac{r}{r_c}) n(r,t) \tag{A3.8}$$

Where $r_c = \frac{e_0^2}{4\pi\varepsilon_0\varepsilon_s k_B T}$ denotes the Onsager radius. The initial condition (for instantaneous RIP generation) is taken to be:

$$n(r, t=0) = \delta(r - r_I) / 4\pi r^2 \tag{A3.9}$$

and the system obeys the radiation boundary condition:

$$\left(\frac{\partial n}{\partial r} + \frac{r_c}{r^2} n - \frac{k_a}{4\pi r_E^2 D(r_E)} n \right)|_{r=r_E} \tag{A3.10}$$

ACRONYMS

Solvents

BN : butyronitrile
DMSO : dimethylsulfoxide
PA : propyl acetate
TOL : toluene

Substances

DMA : *N*,*N*-dimethylaniline
DMAnt : 9,10-dimethylanthracene

Others

A : acceptor
D : donor
ET : electron transfer
F : fluorophore
GS : ground state
HFI : hyperfine interaction
LE : locally excited
LIP : loose ion pair
MFE : magnetic field effect
PET : photo-induced electron transfer
P : product
Q : quencher
R : reactant
RIP : radical ion pair
S : singlet
SRIP : singlet radical ion pair

SS : steady-state

T : triplet

TCSPC : time-correlated single photon-counting

TR : time-resolved

TR-MFE : time-resolved magnetic field effect

REFERENCES

[1] H. M. Hoang, T. B. V. Pham, G. Grampp and D. R. Kattnig, *J. Phys. Chem. Lett.*, 2014, **5**, 3188–3194.

[2] P. Roy, A. K. Jana, G. M.B and D. N. Nath, *Chem. Phys. Lett.*, 2012, **554**, 82–85.

[3] N. K. Petrov, V. N. Borisenko and M. V. Alfimov, *J. Chem. Soc. Faraday Trans.*, 1994, **90**, 109-111.

[4] K. Pal, D. R. Kattnig, G. Grampp and S. Landgraf, *Phys. Chem. Chem. Phys.*, 2012, **14**, 3155-3161.

[5] D. R. Kattnig, A. Rosspeintner and G. Grampp, *Phys. Chem. Chem. Phys.*, 2011, **13**, 3446-3460.

[6] K. Pal, G. Grampp and D. R. Kattnig, *ChemPhysChem*, 2013, **14**, 3389–3399.

[7] D. R. Kattnig, A. Rosspeintner and G. Grampp, *Angew. Chem. Int. Ed.*, 2008, **47**, 960–962.

[8] O. F. Mohammed, K. Adamczyk, N. Banerji, J. Dreyer, B. Lang, E. T. J. Nibbering and E. Vauthey, *Angew. Chem. Int. Ed.*, 2008, **47**, 9044–9048.

[9] T. Inada, K. Kikuchi, Y. Takahashi, H. Ikeda and T. Miyashi, *J. Phys. Chem. A*, 2002, **106**, 4345–4349.

[10] K. Kikuchi, T. Niwa, Y. Takahashi, H. Ikeda, T. Miyashi and M. Hoshi, *Chem. Phys. Lett.*, 1990, **173**, 421–424.

[11] H. Miyasaka, S. Ojima and N. Mataga, *J. Phys. Chem.*, 1989, **93**, 3380–3382.

[12] T. Sengupta, S. Dutta Choudhury and S. Basu, *J. Am. Chem. Soc.*, 2004, **126**, 10589–10593.

[13] K. B. Henbest, P. Kukura, C. T. Rodgers, P. J. Hore and C. R. Timmel, *J. Am. Chem. Soc.*, 2004, **126**, 8102–8103.

[14] K. B. Henbest, P. Kukura, C. T. Rodgers, P. J. Hore and C. R. Timmel, *J. Am. Chem. Soc.*, 2004, **126**, 8102–8103.

[15] C. T. Rodgers, S. A. Norman, K. B. Henbest, C. R. Timmel and P. J. Hore, *J. Am. Chem. Soc.*, 2007, **129**, 6746–6755.

[16] M. Justinek, G. Grampp, S. Landgraf, P. J. Hore and N. N. Lukzen, *J. Am. Chem. Soc.*, 2004, **126**, 5635–5646.

[17] N. N. Lukzen, D. R. Kattnig and G. Grampp, *Chem. Phys. Lett.*, 2005, **413**, 118–122.

[18] S. Aich and S. Basu, *J. Phys. Chem. A*, 1998, **102**, 722–729.

[19] U. Werner and H. Staerk, *J. Phys. Chem.*, 1995, **99**, 248–254.

[20] S. Richert, A. Rosspeintner, S. Landgraf, G. Grampp, E. Vauthey and D. R. Kattnig, *J. Am. Chem. Soc.*, 2013, **135**, 15144–15152.

[21] U. E. Steiner and T. Ulrich, *Chem. Rev.*, 1989, **89**, 51–147.

[22] K. M. Salikhov, I. N. Molin and A. L. Buchachenko, Eds., *Spin polarization and magnetic effects in radical reactions*, Elsevier ; Akadémiai Kiadó, Amsterdam ; New York : Budapest, Hungary, 1984.

[23] G. L. Closs, *J. Am. Chem. Soc.*, 1969, **91**, 4552–4554.

[24] R. Kaptein and J. L. Oosterhoff, *Chem. Phys. Lett.*, 1969, **4**, 195–197.

[25] H. Leonhardt and A. Weller, *Phys. Chem.*, 1961, **29**, 277-281.

[26] H. Knibbe, *J. Chem. Phys.*, 1967, **47**, 1184-1185.

[27] D. N. Nath, S. Basu and M. Chowdhury, *J. Chem. Phys.*, 1989, **91**, 5857-5859.

[28] N. K. Petrov, V. N. Borisenko, A. V. Starostin and M. V. Al'fimov, *J. Phys. Chem.*, 1992, **96**, 2901–2903.

[29] A. Weller, H. Staerk and R. Treichel, *Faraday Discuss. Chem. Soc.*, 1984, **78**, 271-278.

[30] Y. Tanimoto, K. Hasegawa, N. Okada, M. Itoh, K. Iwai, K. Sugioka, F. Takemura, R. Nakagaki and S. Nagakura, *J. Phys. Chem.*, 1989, **93**, 3586–3594.

[31] R. A. Marcus, *J. Chem. Phys.*, 1956, **24**, 966-978.

[32] R. A. Marcus, *J. Chem. Phys.*, 1957, **26**, 867-871.

[33] R. A. Marcus and N. Sutin, *Biochim. Biophys. Acta BBA - Rev. Bioenerg.*, 1985, **811**, 265–322.

[34] P. Siders and R. A. Marcus, *J. Am. Chem. Soc.*, 1981, **103**, 748–752.

[35] Rabinowich, E., *Photosynthesis and related processes***,** Interscience, New York, 1945**.**

[36] H. Leonhardt and A. Weller, *Ber. Bunsen-Ges. Phys. Chem.*, 1963, **76**, 791-795.

[37] G. J. Kavarnos, *Fundamentals of photoinduced electron transfer*, VCH Publishers, New York, NY, 1993.

[38] G. J. Kavarnos and N. J. Turro, *Chem. Rev.*, 1986, **86**, 401–449.

[39] G. Angulo, PhD thesis, Graz University of Technology, 2003.

[40] J. M. Schurr, *Biophys. J.*, 1970, **10**, 700–716.

[41] A. Rosspeintner, PhD thesis, Graz University of Technology, 2008.

[42] E. A. Kotomin, *Modern aspects of diffusion-controlled reactions: cooperative phenomena in bimolecular processes*, Elsevier, Amsterdam ; New York, 1996.

[43] A. Weller, *Pure Appl. Chem.* 1968, **16**, 115-123.

[44] D. Rehm and Weller, A, *Isr. J. Chem.* 1970, **8**, 259-271.

[45] K. Chibisov, *Russ. Chem. Rev. (Engl. Transl.)* 1981, **50**, 1169-1196.

[46] N. Sutin, *Ace. Chem. Res.* 1982, **15**, 275-282.

[47] J. A. McCammon, S. H. Northrup and S. A. Allison, *J. Phys. Chem.*, 1986, **90**, 3901–3905.

[48] R. A Marcus. Nobel lecture, 1992. Chemistry.

[49] R. A. Marcus and P. Siders, *J. Phys. Chem.*, 1982, **86**, 622–630.

[50] H. Staerk, W. Kühnle, R. Treichel and A. Weller, *Chem. Phys. Lett.*, 1985, **118**, 19–24.

[51] A. M. Swinnen, M. Van der Auweraer, F. C. De Schryver, K. Nakatani, T. Okada and N. Mataga, *J. Am. Chem. Soc.*, 1987, **109**, 321–330.

[52] M. R. Wasielewski, D. W. Minsek, M. P. Niemczyk, W. A. Svec and N. C. C. Yang, *J. Am. Chem. Soc.*, 1990, **112**, 2823–2824.

[53] N. Banerji, G. Angulo, I. Barabanov and E. Vauthey, *J. Phys. Chem. A*, 2008, **112**, 9665–9674.

[54] A. Morandeira, A. Fürstenberg and E. Vauthey, *J. Phys. Chem. A*, 2004, **108**, 8190–8200.

[55] Man Him Hui and W. R. Ware, *J. Am. Chem. Soc.*, 1976, **98**, 4718–4727.

[56] I. R. Gould, R. H. Young, L. J. Mueller and S. Farid, *J. Am. Chem. Soc.*, 1994, **116**, 8176–8187.

[57] P.-A. Muller, C. Högemann, X. Allonas, P. Jacques and E. Vauthey, *Chem. Phys. Lett.*, 2000, **326**, 321–327.

[58] H. Hayashi, *Introduction to dynamic spin chemistry: magnetic field effects on chemical and biochemical reactions*, World Scientific, River Edge, N.J, 2004.

[59] E. Vauthey, *J. Phys. Chem. A*, 2001, **105**, 340–348.

[60] M. R. Wasielewski, M. P. Niemczyk, W. A. Svec and E. B. Pewitt, *J. Am. Chem. Soc.*, 1985, **107**, 1080–1082.

[61] N. Mataga, Y. Kanda and T. Okada, *J. Phys. Chem.*, 1986, **90**, 3880–3882.

[62] P. Suppan, *J. Chem. Soc. Faraday Trans. 1 Phys. Chem. Condens. Phases*, 1987, **83**, 495-509.

[63] J. H. Hildebrand and R. Scott, *The solubility of Non-electrolytes*, New York: Reinhold, 1950.

[64] H. F. Herbrandson and F. R. Neufeld, *J. Org. Chem.*, 1966, **31**, 1140–1143.

[65] M. V. Basilevsky, A. V. Odinokov, E. A. Nikitina and N. C. Petrov, *J. Electroanal. Chem.*, 2011, **660**, 339–346.

[66] C. Lerf and P. Suppan, *J. Chem. Soc. Faraday Trans.*, 1992, **88**, 963-969.

[67] N. K. Petrov, *High Energy Chem*. 2006, **40**, 22-34.

[68] N. K. Petrov, A. Wiessner and H. Staerk, *Chem. Phys. Lett.*, 2001, **349**, 517–520.

[69] Y. I. Kharkats, A. A. Kornyshev and M. A. Vorotyntsev, *J. Chem. Soc. Faraday Trans. 2*, 1976, **72**, 361-371.

[70] J. R. Lakowicz, *Principles of fluorescence spectroscopy*, Springer, New York, 3rd ed., 2006.

[71] A. Rosspeintner, D. R. Kattnig, G. Angulo, S. Landgraf, G. Grampp and A. Cuetos, *Chem. - Eur. J.*, 2007, **13**, 6474–6483.

[72] J. Bolton, A. Carrington, A. McLachlan, *Mol. Phys*, 1962, **5**, 31-41.

[73] M. Montalti and S. L. Murov, Eds., *Handbook of photochemistry*, CRC/Taylor & Francis, Boca Raton, 3rd ed., 2006.

[74] Auslander, G. *Br. Chem. Eng*. **1964**, 9, 610.

[75] Ali. A.; Nain. A. K.; Chand. D.; Ahmad. R. Viscosities and refractive indices of binary mixtures of dimethylsulfoxide with some aromatic hydrocarbons at different temperature: an experimental and theoretical study. *J. Chin. Chem. Soc*. **2006**, 53, 531-543.

[76] J. A. Riddick, *Organic solvents: physical properties and methods of purification*, Wiley, New York, 4th ed., 1986.

[77] M. G. Kuzmin, I. V. Soboleva and E. V. Dolotova, *J. Phys. Chem. A*, 2007, **111**, 206–215.

[78] P. Suppan, *J. Photochem. Photobiol. A*, 1990, **50**, 293-330.

[79] D. N. Nath and M. Chowdhury, *Chem. Phys. Lett.*, 1984, **109**, 13–17.

[80] I. R. Gould and S. Farid, *J. Phys. Chem.*, 1992, **96**, 7635–7640.

[81] M. G. Kuzmin, *J. Photochem. Photobiol. Chem.*, 1996, **102**, 51–57.

[82] E. Vauthey, C. Högemann and X. Allonas, *J. Phys. Chem. A*, 1998, **102**, 7362–7369.

[83] E.V. Dolotova, I. V. Soboleva and M. G. Kuzmin, *High Energy Chem*. 2003, **37**, 231-240.

[84] N. K. Petrov, A. Wiessner, T. Fiebig and H. Staerk, *Chem. Phys. Lett.*, 1995, **241**, 127–132.